

Petrology and Geochemistry of lavas from Sal Island: Implications for the variability of the Cape Verde magmatism.

P. TORRES*†; L. C. SILVA*, **; J. MUNHÁ**, ***; R. CALDEIRA*, **, ****¹; J. MATA**, *** & C. TASSINARI*****

Keywords: Cape Verde Archipelago; Mantle plume; EM1; HIMU; Sal Island.

Abstract: Sal Island (Cape Verde Archipelago) preserves a magmatic history ranging from ≈ 25.6 Ma to ≈ 0.6 Ma. The chemistry of magmatism varies from Hy-normative (Serra Negra basalts: ≈ 5 Ma) to highly SiO_2 -undersaturated (nephelinites and melilitites). The calculated temperatures of magmatic segregation are higher than those usually considered for the asthenosphere, thus endorsing the role of a mantle plume to the origin of Cape Verde magmatism. Nephelinites and melilitites are characterized by pronounced K negative anomalies which are interpreted as reflecting the interaction of plume magmas with the lithosphere. Some of the Sal lavas are characterized by low $^{143}\text{Nd}/^{144}\text{Nd}$ (down to 0.512577) – when compared with the HIMU component. These values are similar to those usually reported for the Southern Cape Verde Islands. This suggest the role of a EM1-type end-member to the magma sources of the Sal, which is for the first time evidenced from the whole rock composition of one of the Northern Cape Verde Islands.

Palavras-chave: Arquipélago de Cabo Verde, Pluma mantélica, EM1, HIMU; Ilha do Sal.

Resumo: A ilha do Sal (Arquipélago de Cabo Verde) preserva uma história magmática estendendo-se desde os ≈ 25.6 Ma aos ≈ 0.6 Ma. As características químicas do magmatismo variam desde composições caracterizadas por hiperstena normativa, em rochas com cerca de 5 Ma (Formação da Serra Negra), até litótipos altamente subsaturados em sílica (nefelinitos e melilititos). As temperaturas de extracção magmática calculadas indicam valores superiores aos normalmente referenciados para a astenosfera, suportando os modelos que invocam o papel de uma pluma mantélica para a origem dos magmas de Cabo Verde. Nefelinitos e melilititos caracterizam-se por pronunciadas anomalias negativas em K que são interpretadas como resultado da interacção dos magmas provenientes da pluma mantélica com a litosfera. Algumas das lavas da ilha do Sal caracterizam-se por valores de $^{143}\text{Nd}/^{144}\text{Nd}$ baixos (até 0.512577) quando comparados com os que caracterizam o componente HIMU. Tais características são similares às que têm sido descritas para as ilhas de Sul. Tal indica que, em oposição ao normalmente considerado, a contribuição do componente EM1 para as fontes mantélicas de Cabo Verde não se restringe às ilhas do Sul.

1 – INTRODUCTION

Cape Verde archipelago ($14^{\circ}48' - 17^{\circ}12'\text{N}$; $22^{\circ}44' - 25^{\circ}28'\text{W}$) is located on the East Central Atlantic between the Equator and the Cancer Tropic, some 600 to 900 km away from the western African coast and ≈ 2000 km to the east of the Mid Atlantic Ridge.

The archipelago (Fig. 1) is composed of two groups of islands (windward vs. leeward or Northern vs. Southern), a subdivision that also reflects their different geochemical characteristics. Southern Islands are less Nd- and Pb-radiogenic and more Sr-radiogenic than the Northern Islands, which are also characterised by more unradiogenic He signatures. Such distinction is also

* Centro de Geologia, Instituto de Investigação Científica Tropical (IICT)

** Centro de Geologia da Universidade de Lisboa (CeGUL)

*** Faculdade de Ciências da Universidade de Lisboa – Departamento de Geologia (GeoFCUL)

**** U. Geologia e Cartografia Geológica do Laboratório Nacional de Energia e Geologia (LNEG)

***** Centro de Pesquisas Geocronológicas (CPGeo) do Instituto de Geociências do Instituto de Geociências da Universidade de São Paulo (IGc-USP)

¹ Corresponding author: rita.caldeira@ineti.pt

† Deceased

evident from a $^{206}\text{Pb}/^{204}\text{Pb}$ vs. $^{208}\text{Pb}/^{204}\text{Pb}$ diagram. Whereas the Northern Islands plot along the North Hemisphere Reference Line (NHRL; HART, 1984) the Southern Islands are mainly positioned above the NHRL. This dichotomy is considered to reflect the distinct contribution of HIMU- and EM1-type mantle end-members to the sources of these two groups of islands. On Southern Islands an EM1-type end-member dominates whereas on the Northern Islands the isotopic signatures are dominated by a HIMU-type end-member, flavoured with a contribution of the lower mantle in order to account for the unradiogenic He isotopic signatures. The additional contribution of a depleted end-member is mainly required to explain the composition of Northern Islands (GERLACH *et al.*, 1988; DAVIES *et al.*, 1989; CHRISTENSEN *et al.*, 2001; JØRGENSEN & HOLM, 2002; DOUCELANCE *et al.*, 2003; ESCRIG *et al.*, 2005; HOLM *et al.*, 2006; MILLET *et al.*, 2008; BARKER *et al.*, 2009a, b; MARTINS *et al.*, 2010). For submarine lavas of the Flamengos formation (Santiago Island) it was also proposed the contribution of a FOZO-like component (BARKER *et al.*, 2009a; b).

We would like to emphasize that such geochemical distinction between Northern and Southern Islands has been made based upon the study of an incomplete set of data. Indeed, and particularly in what concerns Sal Island, the available isotope data is limited to $^{87}\text{Sr}/^{86}\text{Sr}$ and Pb isotopic ratios for one and three samples, respectively (DOUCELANCE *et al.* 2003).

In this paper we will present detailed geochemical data from Sal Island lavas, which will be discussed in conjunction with the available cartographic (SILVA *et al.*, 1990) and geochronological (TORRES *et al.*, 2002a; HOLM *et al.*, 2008) data.

2 – GEOLOGICAL SETTING

The Cape Verde archipelago occurs on an ≈ 83 km thick lithosphere (CAZENAVE *et al.*, 1988) with 120 to 140 Ma (WILLIAMS *et al.*, 1990; MÜLLER *et al.* 2008) and is composed by 10 islands and 8 islets presenting a horse-shoe geographical distribution opening westward. It is

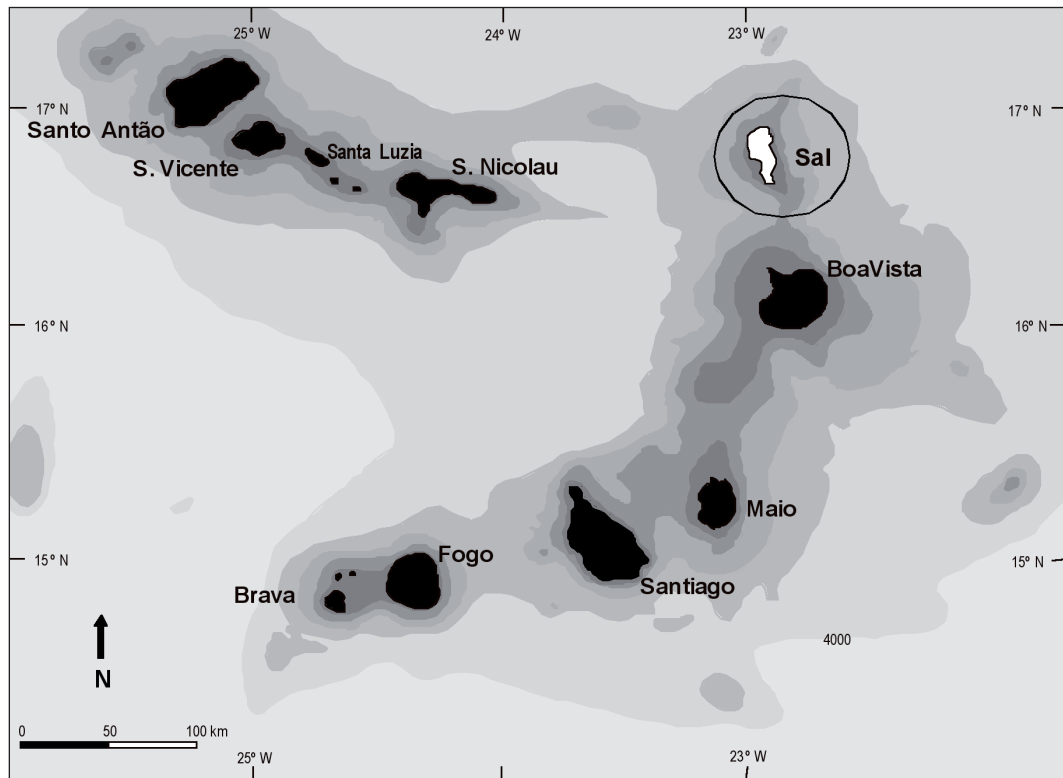


Fig. 1 – Location of Sal Island at the Cape Verde Archipelago.

located on the southwest part of the Cape Verde Rise, a ≈ 2.2 km high and 1400–1600 km wide swell considered the largest oceanic intraplate bathymetric anomaly (e.g. LODGE & HELFFRICH, 2006). Crustal thickness is anomalously high (up to 22 km) beneath the islands, which is attributed to magmatic transfer from the mantle plume source to crustal levels (LODGE & HELFFRICH, 2006). However, between the islands the crust is only ≈ 7 km thick, which is normal for oceanic settings (ALI *et al.*, 2003; PIM *et al.*, 2008).

The positioning of the Cape Verde archipelago is also coincident with important geoid (7.6 ± 0.3 m) and heat flow (16 ± 4 mWm $^{-2}$) anomalies (COURTNEY & WHITE, 1986; MONNEREAU & CAZENAVE, 1990) being characterized by a geoid height to topography ratio (4.4 ± 0.23) consistent with the reheating of the lower lithosphere (GREVEMEYER, 1999). The Cape Verde islands are flanked by a flexural moat, which is less important than it would be expected from surface volcanic(s) loading. This was interpreted as suggesting the existence of subsurface, upward acting, loads counteracting that surface downward loading (ALI *et al.*, 2003). All these suggest the role of a mantle plume to the genesis of Cape Verde.

The genesis of Cape Verde from a deeply anchored mantle plume seems to be supported by seismic tomography studies imaging a low S-wave velocity domain extending down to 2800 km (MONTELLI *et al.*, 2006; see also ZHAO, 2007) and by unradiogenic He isotope signatures obtained both from silicate and carbonatitic rocks (R/Ra up to 15), which point to the contribution of a high $^3\text{He}/^4\text{He}$ reservoir, plausibly located in the deepest parts of the lower mantle (cf. CHRISTENSEN *et al.*, 2001; DOUCELANCE *et al.*, 2003; MOURÃO *et al.*, 2007; MATA *et al.*, 2010). However, a recent analysis of P-to-S receiver functions showed that the time separation between the 410 and 660 km discontinuities is not modified beneath Cape Verde (HELFFRICH *et al.*, 2010), suggesting that the plume role on the magma genesis is still an open question in Cape Verde.

The region has been subjected to very important vertical movements testified by the occurrence of MORB at Maio and Santiago islands (DE PAEPE *et al.*, 1974; GERLACH *et al.*, 1988; MILLET *et al.*, 2008), by seafloor sediments of disputable Lower Cretaceous age cropping out in Maio (e.g. AZÉMA *et al.*, 1990; HOLM *et al.*, 2008) and by the occurrence on several islands of uplifted submarine alkaline lavas, which, for example, reach 450 m apsl in Santiago Island and 400 m apsl in Brava Island (SERRALHEIRO, 1976; ZAZO *et al.*, 2007; HOLM *et al.*,

2008; RAMALHO *et al.*, 2010 a; b; MADEIRA *et al.*, 2008; 2010; MOURÃO *et al.*, 2010).

3 – GEOLOGY AND GEOCHRONOLOGY

With 216 km 2 , Sal is an arid, highly eroded and flat island reaching the highest height at Monte Grande (406 m), a Quaternary lapilli cone.

Extensive field work and K-Ar determinations (TORRES *et al.*, 2002a, see Figs. 2 and 3) enabled the proposition of the following volcanostratigraphic subdivisions (see also TORRES *et al.*, 2002b and HOLM *et al.*, 2008).

The Old Eruptive Complex is mainly composed by submarine lavas and hialoclastites of alkali basaltic composition. The unaltered core of a pillow lava allowed the determination of a reliable K-Ar age of 25.6 Ma (TORRES *et al.*, 2002a) corresponding to the most ancient isotopic age obtained for the Cape Verde hotspot. These rocks were intruded by an impressive dyke swarm of variable composition (basaltic to trachytic) with N70°E, E-W and N20°W as dominant strikes. N70°E is the dominant orientation to the north of the Leteu rivulet, where dykes correspond to about 80 % of the outcropping area. N20°W is the dominant dyke orientation in the region between Madama de Baixo and Madama de Cima rivulets (Fig. 2).

Intrusives bodies (foidic syenites, gabbros and alkali pyroxenites) which sometimes occur as zoned subcircular complexes, are interpreted as resulting from the solidification of subvolcanic magma chambers. In these subsuperficial reservoirs basic Ne-normative magmas gave origin to pyroxenitic cumulates and chemically evolved to produce (theralitic) gabbros, essexites and nepheline syenites (SILVA, 1991, CALDEIRA & SILVA, 2008).

Micritic limestones included in the volcanic products of this complex (SILVA *et al.* 1990; UBALDO *et al.* 1991) attests to the submarine origin of part of the sequence. Furthermore, according to RAMALHO *et al.* (2010 a), the high planktic/benthic ratio indicates pelagic conditions associated with depths in excess of 300–400 m, suggesting that the Old Eruptive Complex corresponds to the seamount stage of the Sal development and implying a significant (> 350 m) uplift of the volcanic island.

Subaerial volcanism is testified by some rare and volumetrically unimportant flows and dykes of melanephelinites and by flows, dykes and chimneys of phonolitic composition.

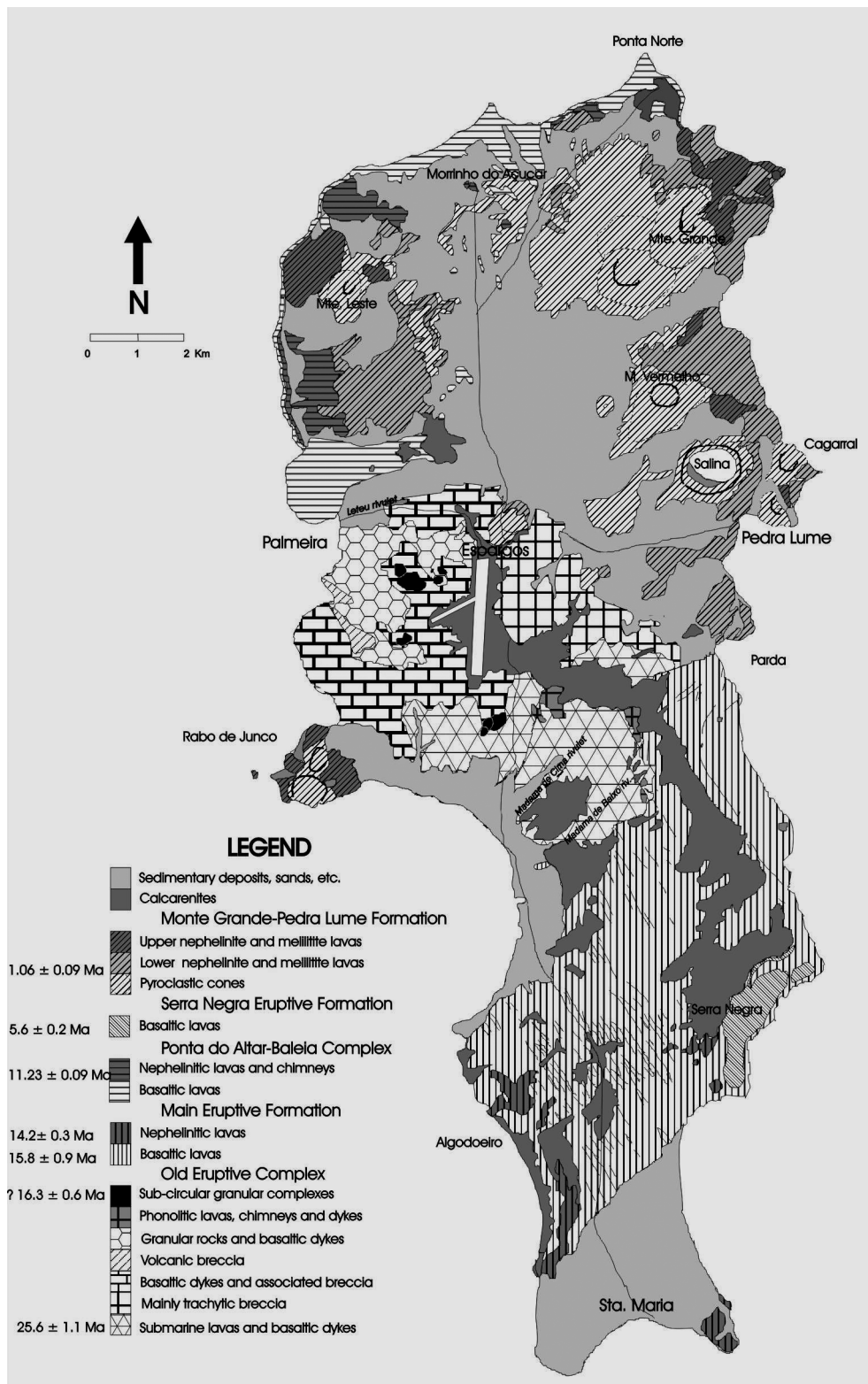


Fig. 2 – Geological map of Sal Island showing the stratigraphic units (after TORRES *et al.*, 2002a), simplified and adapted from “Carta Geológica da ilha do Sal, na escala 1/25 000” (SILVA *et al.*, 1990).

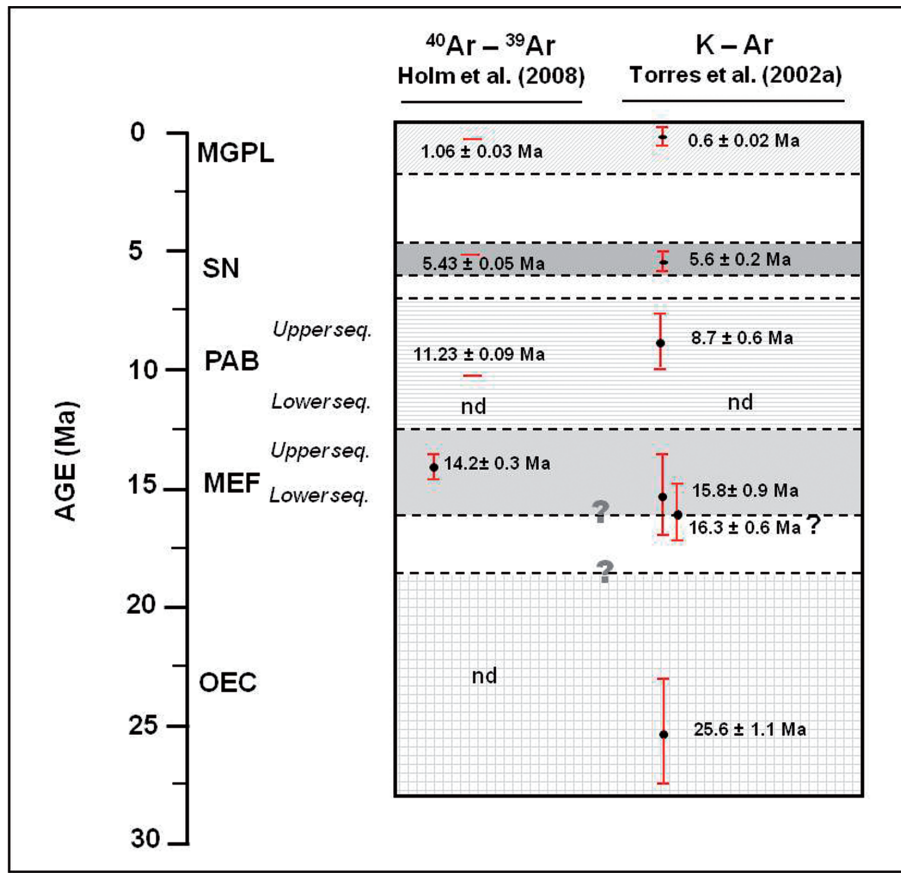


Fig. 3 – Illustration of the available age determinations for Sal Island (TORRES *et al.*, 2002a; HOLM *et al.*, 2008). OEC – Old Eruptive Complex, MEF – Main Eruptive Formation, PAB – Ponta Altar Baleia Complex, SN – Serra Negra Formation, MGPL – Monte Grande Pedra Lume Formation. Black question mark indicates that the age obtained for the essexitic rock of a subcircular complex, thought to be part of the OEC, is close to the age determined for basalts from the MEF. This raises the possibility that some of the intrusives in OEC are coeval with the overlying volcanic sequences, as suggested by TORRES *et al.* (2002a). However, field evidences and a possible age resetting must be taken in consideration. Hence the doubt about the stratigraphic position of these intrusives remains until further age determinations are obtained.

After a period of intense dissection, the eruption rates reached its highest values during the genesis of the **Main Eruptive Formation** when submarine and subaerial alkali olivine basalts (15.8 Ma, TORRES *et al.*, 2002a) and olivine nephelinites (14.2 Ma; HOLM *et al.*, 2008) were formed. This sequence, mainly outcropping in the Southeastern part of the island is followed by the **Ponta do Altar-Baleia Complex**. In this complex, a marine deposit ($\approx 2\text{ m}$ thick), including calcarenites, a conglomeratic level and, towards the top, siltites and argillites, separates the underlying alkali basaltic rocks from the olivine nephelinites. For the upper nephelinitic rocks, outcropping at Morrinho do Açúcar volcanic chimney, ages of 8.7 Ma (TORRES *et al.*, 2002a) and of 11.2 Ma (HOLM *et al.*, 2008) were obtained.

It is worthwhile to notice that TORRES *et al.* (2002a) obtained 9.7 Ma for a nephelinite outcropping in the Serra Negra region, which was considered, by field arguments, to be part of the Main Eruptive Formation (upper sequence). This formation also outcrops on the southeastern extreme of the island where HOLM *et al.* (2008) obtained the $^{40}\text{Ar}/^{39}\text{Ar}$ age of 14.2 Ma. Such significant age discrepancy and the fact that the 9.7 Ma age was obtained from a nephelinite cut by latter ijolitic pegmatitoids, advise for the necessity of an age confirmation for the Main Eruptive Formation nephelinites.

After the formation of these nephelinitic rocks, volcanic activity decreased significantly or even stopped. During this period of volcanic quiescence erosion was the main shaping process of the island being testified by

the formation of a lahar type deposit. During this period marine limestones and calcarenites were also deposited. The study of planctonic foraminiferous allows considering the limestones of an Upper Miocene age (M. Lourdes Ubaldo, oral com.) which conforms with the radiometric ages of the enclosing volcanic rocks. The Main Eruptive Formation is cut by a prominent dyke swarm of a remarkably constant orientation ($N40^{\circ}W$) suggestive of the existence of a clearly anisotropic stress field with σ_1 (compression) oriented to $N40^{\circ}W$.

A new period of volcanic activity occurred by the end of Miocene with the genesis of the **Serra Negra Eruptive Formation** (~ 5.5 Ma; TORRES *et al.*, 2002a; HOLM *et al.*, 2008) in which submarine volcanic facies are gradually replaced by subaerial ones. This is the only period marked by the formation of Hy-normative basaltic rocks at the Sal Island. In opposition with the dominant fissural volcanism during the development of the Old Eruptive Complex and the Main Eruptive Formation, volcanic activity is now clearly centered.

A long period of volcanic quiescence (≈ 5 Ma) occurred until the upper Pleistocene when highly undersaturated rocks (olivine nephelinites and olivine melilitites) were erupted (lava flows and pyroclastic cones) to give origin to the **Monte Grande-Pedra Lume Formation** (1.06 to 0.6 Ma, HOLM *et al.*, 2008; TORRES *et al.*, 2002a). An 1100 m diameter crater generated by a phreatic/phreatomagmatic explosion (SILVA *et al.*, 2002) is the most significant geomorphological expression of this formation; the evaporitic salt deposits continuously forming within it are clearly related with the name of the Sal island. The cones from which the Pedra Lume volcanics erupted occupy a belt limited by the fault zone of Madama de Baixo rivulet. This belt, with a orientation of NE – SW, probably extend seaward as it is suggested by the submarine apron evident from bathymetry of the NNE extremity of the island.

The highly eroded and low-lying morphology of Sal is dominated by extensive wave-cut platforms and terraces mostly formed during Quaternary (BEBIANO 1932; LECOINTRE 1963; SERRALHEIRO 1968; SILVA *et al.*, 1990; TORRES *et al.*, 2002b, ZAZO *et al.*, 2007). Recently ZAZO *et al.*, (2007) identified 16 terrace levels from 1 to 60 m a.s.l. but, as noticed by RAMALHO *et al.* (2010a), omitted the 100 m level, on top of Serra Negra, previously identified by SILVA *et al.* (1990). According to RAMALHO *et al.* (2010a), this terrace is older than 1 Ma.

4 – ANALYTICAL METHODS

A subset of 58 samples were selected for analysis from a larger collection taking in account the defined volcanostratigraphy and a careful thin section study (which screened out samples presenting strong evidences of meteoric/hydrothermal alteration and/or where phenocrysts represent $> 10\%$ volume). These rocks were analyzed for major and trace elements (Cr, Ni, Cu, Zn, Rb, Ba, Sr, Nb, Zr, and Y) at the CCM – IICT (Centro de Cristalografia e Mineralogia do Instituto de Investigação Científica Tropical, Portugal) by X-ray fluorescence spectrometry (Philips PW 1400). 18 samples were further analyzed for REE (and Sc, Cs, Ta, Hf, and U) by neutron activation (INAA) at the Activation Laboratories LTD (Ontario, Canada) and for $^{87}\text{Sr}/^{86}\text{Sr}$ and $^{143}\text{Nd}/^{144}\text{Nd}$ at the CPGeo-IGUSP (Centro de Pesquisas Geocronológicas do Instituto de Geociências da Universidade de São Paulo, Brasil).

Sm-Nd analytical procedures followed those described by SATO *et al.* (1995).

Mass spectrometric analyses were performed on a VG ISOMASS 354 fully automated mass spectrometer with five collectors. Sm and Nd analysis were determined by isotopic dilution technique, using a mixed $^{149}\text{Sm}-^{150}\text{Nd}$ spike, with an Nd concentration of 0.0003314 mmol/g and ^{149}Sm content of 0.004575 mmol/g. Nd and Sm were loaded as phosphates on two Ta side filaments of a triple filament assembly, with Re as the ionizing central filament. The quality of the analytical measurements by isotopic dilution techniques was evaluated using a standard $^{142}\text{Nd}/^{144}\text{Nd}$ ratio of 1.141828. The Nd isotopic compositions were corrected for mass fractionation by normalizing to a value of 0.7219 for $^{146}\text{Nd}/^{144}\text{Nd}$.

Average $^{143}\text{Nd}/^{144}\text{Nd}$ for La Jolla and BCR-1 standards, yielded results of 0.511847 ± 0.000022 and 0.512662 ± 0.000027 , respectively.

Rb and Sr contents and Rb/Sr ratios were determined by X-Ray fluorescence on powders by means of a Philips PW- 1380/00 automatic spectrometer. Samples with low Rb and Sr contents (2ppm), were re-analyzed by isotopic dilution technique, using ^{85}Rb and ^{84}Sr spikes. The samples were dissolved with $\text{HF}+\text{HNO}_3$ overnight at 65°C , and the Sr purified using a conventional ion exchange column with AG50WX8 cation exchange resin (200-400#) as described, with some modifications, by KAWASHITA (1972). The Sr was loaded on a single Ta filament with phosphoric acid. The $^{87}\text{Sr}/^{86}\text{Sr}$ ratios were corrected for mass fractionation by normalizing to a

value of 0.1194 for $^{86}\text{Sr}/^{88}\text{Sr}$. During the period of this work, six analyses of the NBS-987 standard averaged 0.71026 ± 0.00002 (Is). Procedural blanks for Sr were of the order of 1 ng. Errors reported here for initial $^{87}\text{Sr}/^{86}\text{Sr}$ ratios (ISr) are at the 2s level.

Mineral compositions were determined at Centro de Geologia da Universidade de Lisboa (CeGUL), on polished thin sections, using a 5 μm beam in a three channel wavelength dispersive JEOL-JCXA733 electron microprobe, operated at an accelerating voltage of 15 kV and a probe current of 25 nA. Standards were natural homogeneous minerals (Si-wollastonite and olivine; Ca-wollastonite; Ti and Na – kaersutite; Ti – ilmenite; Al-disthene; Fe and Mg – olivine; Mn-rhodonite; k-adularia) and synthetic minerals of Cr, V and Ni. Precision, as indicated by replicate determinations on an in-house standard, is better than 2% for major elements. The mineral chemistry data base was recently slightly enlarged with the addition of few analyses made at CeGUL on a JEOL JXA 8200 microprobe, equipped with 4 wave-length dispersive spectrometers (WDS) and an energy dispersive detector (EDS), using a range of natural minerals as standards. An accelerating voltage of 15 kV was combined with a beam current of 10 nA and a beam diameter of 5 μm .

5 – PETROGRAPHY AND MINERAL CHEMISTRY

5.1 Petrography

The main lithotypes representing Sal island lavas are alkali basalts, nephelinites and melilitites.

Alkali basalts are hypocrystalline to holocrystalline, mainly porphyric but occasionally aphyric rocks, frequently with vesicles filled with zeolites or carbonates. Olivine is the main phenocryst phase followed by subordinate clinopyroxene. Plagioclase is rare and amphibole occurs as a phenocryst phase in basalts from the Main Eruptive Formation. Euhedral to subeuhedral olivine (Fo_{62-87}), up to 8 mm across, often displays alteration to iddingsite and/or iron oxides/hydroxides along cracks. Occasionally they exhibit skeletal morphology indicating high growing rates stemming from the swiftness of quenching processes. Purple-brownish Ti-augite (< 1.5 mm across; $\text{Wo}_{48-52}\text{En}_{36-43}\text{Fs}_{9-12}$) frequently display zoning marked by a core to rim Ti enrichment (e.g. TiO_2 from 1.79 to 2.42 wt%). Hourglass-type zoning is occasionally present. Plagioclase, when

present, may reach up to 1.5 mm across, and show core-rim zoning from An_{73} to An_{57} . Amphibole is anhedral, pleochroic, frequently with reabsorbed rims where opaque minerals dominate. This is interpreted as the result of destabilization of amphibole due to devolatilization affecting magma during ascent. The groundmass in alkali basalts invariably consists of plagioclase laths ($65.21 - 48.84$ mol % An), occasionally oriented, Ti-augite ($\text{Wo}_{48-50}\text{En}_{33-41}\text{Fs}_{11-17}$; $\text{TiO}_2 \approx 5.19$ wt%), and opaque oxide grains. Olivine may also occur. Interstitial brown isotropic glass is present in the groundmass of submarine lavas. Serra Negra Formation hyaloclastites locally show signs of phosphatization, demonstrated by the presence of phosphate minerals predominantly of the variscite type (SILVA *et al.*, 1993).

Nephelinites and melilitites are holocrystalline, porphyric, sometimes with glomeroporphyritic texture. The phenocrystal assemblage comprises olivine (Fo_{81-87}), clinopyroxene and opaque minerals. Olivine (up to 5 mm), sometimes with primary fluid inclusions, is frequently altered to iron oxides/hydroxides and serpentine. Some olivines display kink-bands (indicating deformation inside a solid matrix), allowing the interpretation that they correspond xenocrystals derived from xenoliths desegregation. The main clinopyroxene type is Ti-augite ($\text{Wo}_{51-54}\text{En}_{31-40}\text{Fs}_{10-15}$; $\text{TiO}_2 = 6.33 - 7.25$ wt %), up to 2.5 mm across and sometimes with hourglass zoning. Ti-augites are sometimes totally or partially replaced by crystal aggregates of yellowish-green esseñites ($\text{Wo}_{57-70}\text{En}_{29-36}\text{Fs}_{7-0.7}$; $\text{TiO}_2 = 0.23 - 1.99$ wt %) that were interpreted as result of subsolidus fluid/rock interaction under high oxygen fugacity conditions (MUNHÁ *et al.*, 1991). The groundmass includes olivine, variable amounts of clinopyroxene ($\text{Wo}_{51-54}\text{En}_{34-39}\text{Fs}_{9-12}$), nepheline (sometimes in interstitial poecilitic crystals), melilite ($\text{Aker}_{66}\text{Gehl}_{34}$; elongated microliths frequently altered and displaying typical peg-structure), perowskite, biotite/phlogopite and Fe-Ti oxides. Some samples have ocelli-like vesicles filled with carbonates and zeolites. Flakes of dark-red rhönite and small crystals of hauyne are present in the matrix of some olivine melilitites from the Monte Grande – Pedra Lume Formation. Variable proportions of clinopyroxene, nepheline and melilite in the groundmass lead to transitions between olivine melanephelinites, olivine nephelinites with melilite, and olivine melilitites.

Mantle xenoliths such as dunite/wherlite cumulates and lherzolite/harzburgite refractory residues are present in nephelinitic and alkali basaltic lavas (DE PAEPE &

KLERKX, 1971; KOGARGO & SENIN, 1993; RYABCHIKOV *et al.*, 1995; BONADIMAN *et al.*, 2005; MENDES *et al.*, 2005; SHAW *et al.*, 2006). Gabbro and gabbronorite xenoliths included in olivine melanephelinites from Monte Grande – Pedra Lume Formation were interpreted as representing fragmental pieces of the oceanic crust crossed by ascending magmas (MENDES & SILVA, 2001).

5.2 Mineral Chemistry

Representative electron microprobe analyses of phases in the volcanic rocks from Sal Island are given in tables 1 – 6.

Olivine is compositionally variable with Fo contents ranging from 62 to 87 mol %, MnO from 0.11 to 0.77 wt%, CaO from 0.15 to 1.01 wt %, and NiO from 0.01 to 0.45 wt%. Olivine in nephelinitic/melilitic rocks tends to have lower NiO concentration at a given Fo, when compared to basaltic olivines. Phenocrysts are usually zoned, with Fo and Ni decreasing and Ca and Mn increasing from core to rim. The increase of Ca content normally is attributed to a response to pressure decrease during magma ascent (HIRSCHMANN & GHIORSO, 1994). However, the distinct evolutionary trends displayed by olivine in basaltic and nephelinitic rocks (Fig. 4) show that the composition of olivine is also strongly dependent of magma composition and crystallization temperature. Indeed it has been

suggested that CaO content of olivines varies inversely with silica activity whereas $D_{Ni}^{ol/liq}$ increases with the decrease of polymerization degree of the magma (e.g. WATSON, 1979; MATA, 1996; 1998). This is supported by the Sal data depicted in Fig. 6 taking into account that SiO₂ range from 39 to 45 wt% in basalts and from 34 to 40 wt % in nephelinites (see table 7).

Estimation of olivine phenocrysts crystallization temperatures by the methods of ROEDDER & EMSLIE (1970) and BEATTIE (1993), indicates values from 1266 to 1326 °C for basaltic rocks and 1324 to 1363 °C for nephelinites/melilitites. For these calculations only olivine-whole rock pairs for which $K_{D_{Fe/Mg}^{ol/liq}} \approx 0.30$ were used in order to ensure that crystal/liquid equilibrium was attained (ROEDDER & EMSLIE, 1970).

Most **pyroxenes** found in Sal Island basaltic and nephelinitic lavas are classified as diopsides although in many of the nephelinitic/melilitic rocks they have Wo > 50 mol %, as it is typical for silica-undersaturated lavas. Some of the pyroxenes in nephelinites/melilitites are esseneites resulting from low-temperature recrystallization of diopsides (MUNHÁ *et al.*, 1991). Diopsidic clinopyroxenes are enriched in Al₂O₃ and TiO₂ (up to 10.85 and 6.65 wt % respectively) with the highest concentrations confined to the rims and groundmass. Diopsides are Ca rich (CaO = 21 to 25 wt %) showing a general increase from alkali basalts (Ca < 0.94 a.f.u.) to

TABLE 1
Representative olivine microprobe analyses of Sal lavas

Geol Unit	Main Eruptive Formation				Ponta do Altar Baleia				Serra Negra				Monte Grande - Pedra Lume								
	Basanite		Nephelinite		Basanite		Basanite		Nephelinite		Basanite		Basanite		Basanite		Nephelinite		Nephelinite		
	C	R	C	R	C	R	C	R	C	R	C	R	C	I	R	C	R	C	R	C	R
SiO ₂ (wt %)	37.08	36.55	39.80	39.54	39.70	39.20	39.96	39.36	40.15	39.58	40.44	39.28	40.25	39.77	39.64	39.89	38.80	40.40	39.80	40.31	39.73
TiO ₂	0.06	0.06	0.04	0.00	0.00	0.06	0.02	0.01	0.05	0.02	0.01	0.02	0.03	0.01	0.03	0.03	0.07	0.04	0.03	0.05	0.04
Al ₂ O ₃	0.02	0.04	0.04	0.00	0.04	0.00	0.05	0.03	0.05	0.02	0.02	0.04	0.03	0.02	0.04	0.05	0.05	0.06	0.02	0.03	0.03
NiO	0.06	0.03	0.11	0.10	0.20	0.14	0.25	0.15	0.24	0.04	0.27	0.18	0.28	0.29	0.21	0.27	0.10	0.23	0.14	0.26	0.08
FeO	29.56	32.15	14.79	15.98	14.51	19.46	15.24	16.35	12.93	14.10	13.59	16.48	12.96	13.34	14.45	13.58	21.63	12.99	13.50	12.42	13.66
MnO	0.66	0.77	0.33	0.42	0.21	0.24	0.20	0.25	0.20	0.49	0.18	0.28	0.18	0.19	0.19	0.21	0.33	0.17	0.22	0.17	0.39
MgO	31.80	29.72	44.02	43.35	44.68	40.33	44.29	43.37	46.54	43.78	45.86	42.73	46.58	46.29	44.63	45.60	38.33	46.02	45.66	46.74	44.96
CaO	0.45	0.53	0.46	0.69	0.25	0.36	0.22	0.36	0.19	0.99	0.22	0.29	0.20	0.23	0.34	0.24	0.49	0.13	0.25	0.15	0.73
Total	99.68	99.85	99.59	100.08	99.60	99.79	100.23	99.89	100.35	99.03	100.60	99.29	100.50	100.15	99.53	99.87	99.79	100.03	99.62	100.12	99.62
% Fo	65.73	62.24	84.14	82.87	84.59	78.69	83.82	82.54	86.52	84.70	85.75	82.22	86.50	86.09	84.63	85.68	75.96	86.33	85.77	87.03	85.43
% Fa	34.27	37.76	15.86	17.13	15.41	21.31	16.18	17.46	13.48	15.30	14.25	17.78	13.50	13.91	15.37	14.32	24.04	13.67	14.23	12.97	14.57
Si ⁴⁺	1.006	1.003	1.004	0.999	1.000	1.008	1.003	0.998	0.996	1.003	1.003	1.002	0.997	0.992	0.999	0.998	1.008	1.004	0.997	0.999	0.998
Ti ⁴⁺	0.001	0.001	0.001	0.000	0.000	0.001	0.000	0.000	0.001	0.000	0.000	0.000	0.001	0.000	0.001	0.000	0.001	0.001	0.001	0.001	0.001
Al ³⁺	0.001	0.001	0.001	0.000	0.001	0.000	0.002	0.001	0.001	0.001	0.001	0.001	0.001	0.001	0.001	0.001	0.002	0.002	0.000	0.001	0.001
Ni ²⁺	0.001	0.001	0.002	0.002	0.004	0.003	0.005	0.003	0.005	0.001	0.006	0.006	0.004	0.005	0.004	0.005	0.002	0.005	0.003	0.005	0.002
Fe ²⁺	0.670	0.738	0.312	0.338	0.306	0.418	0.320	0.347	0.268	0.299	0.282	0.351	0.269	0.278	0.304	0.284	0.470	0.270	0.283	0.257	0.287
Mn ²⁺	0.015	0.018	0.007	0.009	0.004	0.005	0.004	0.005	0.004	0.011	0.004	0.006	0.004	0.004	0.005	0.005	0.007	0.004	0.005	0.004	0.008
Mg ²⁺	1.286	1.217	1.655	1.634	1.677	1.546	1.657	1.638	1.721	1.655	1.696	1.625	1.720	1.721	1.677	1.701	1.485	1.706	1.706	1.728	1.684
Ca ²⁺	0.013	0.016	0.013	0.019	0.007	0.010	0.006	0.010	0.005	0.027	0.006	0.008	0.005	0.006	0.009	0.006	0.014	0.004	0.007	0.004	0.020

C – core, R – rim, I – intermediate zone. For the complete set of analyses see Torres (1998).

TABLE 2
Representative clinopyroxene microprobe analyses of Sal lavas

Geo Unit	Main Eruptive Formation						Serra Negra						Porto do Alter Balao						Monte Graciosa Peda-Lume												
	Basalt			1025			Basalt			Basalt			Basalt			Nephelinitic			Nephelinitic			Nephelinitic									
	C	I	R	M	C	I	M	C	I	M	C	R	M	C	I	R	M	C	I	R	M	C	I	R	M						
SiO ₂ wt%	50.32	48.92	47.53	46.39	44.76	48.39	48.73	44.72	46.36	47.29	45.18	49.59	50.66	49.21	49.16	49.84	49.25	48.63	43.61	46.29	47.93	48.30	40.31	42.89	43.59	47.38	40.45	50.43	44.27	38.26	
TiO ₂	1.23	1.49	2.25	2.51	3.74	2.15	2.06	4.37	3.12	2.51	2.39	1.79	1.55	2.42	1.83	1.64	1.61	3.20	3.99	2.79	2.88	2.72	5.83	4.44	4.01	2.89	6.65	2.34	10.85	2.87	0.23
Al ₂ O ₃	4.59	5.41	6.41	7.20	7.43	4.30	4.05	6.75	6.57	6.07	6.73	5.13	3.79	4.57	4.90	4.21	4.42	5.26	9.73	7.26	5.38	4.59	4.59	10.28	8.56	8.09	4.68	13.74	7.62	13.74	
Cr ₂ O ₃	0.22	0.31	0.25	0.20	0.04	0.08	0.16	0.00	0.49	0.30	0.03	0.66	0.43	0.03	0.31	0.32	0.34	0.00	0.52	0.40	0.00	0.00	0.00	0.00	0.04	0.03	0.05	nd.	0.01	nd.	
Fe ₂ O ₃ #	1.69	2.67	3.13	2.98	3.06	2.21	2.51	3.61	1.56	2.26	4.00	0.73	0.48	1.46	2.14	0.50	1.13	1.43	2.08	2.99	0.35	0.67	4.57	4.08	5.34	4.01	4.20	0.43	11.09	15.31	
FeO #	3.84	3.28	3.14	3.77	5.94	5.55	5.06	4.84	5.47	4.79	4.83	5.45	5.47	6.74	4.38	5.73	5.11	10.21	5.05	3.92	8.40	9.28	2.63	1.58	1.98	2.20	4.79	2.50	0.32		
MnO	0.08	0.06	0.06	0.07	0.11	0.13	0.13	0.15	0.11	0.09	0.17	0.11	0.12	0.15	0.10	0.09	0.11	0.16	0.05	0.08	0.18	0.22	0.06	0.04	0.09	0.03	0.08	0.10	0.18		
Mg#	14.82	14.36	13.43	12.84	11.27	14.02	13.89	11.73	12.67	12.57	12.20	13.76	14.46	12.74	13.90	13.82	11.51	11.26	12.69	11.69	10.96	10.15	11.48	11.81	13.46	13.65	9.30	7.23			
CaO	23.02	23.07	23.46	22.92	22.38	21.50	22.20	22.25	22.61	22.99	21.97	22.74	22.68	23.18	23.20	22.99	20.77	22.71	23.37	22.44	23.80	23.41	24.19	24.31	23.98	24.38	24.34	23.98			
Na ₂ O	0.31	0.29	0.36	0.35	0.48	0.33	0.36	0.64	0.24	0.29	0.45	0.35	0.33	0.40	0.32	0.19	0.18	0.23	0.31	0.28	0.36	0.37	0.47	0.45	0.44	0.42	0.41	0.40	0.38	0.36	
K ₂ O	0.01	0.00	0.00	0.00	0.02	0.01	0.01	0.00	0.01	0.00	0.02	0.01	0.01	0.01	0.00	0.01	0.01	0.02	0.01	0.02	0.01	0.00	0.00	0.01	0.01	0.03	0.02	0.06			
Total	100.13	99.86	100.02	99.24	99.18	98.68	99.17	99.07	98.63	98.56	99.18	99.09	99.99	100.81	100.22	99.54	99.07	98.43	99.31	100.07	99.62	100.08	98.09	99.13	98.27	100.22	99.42	100.46	99.66		
Si%	1.851	1.809	1.763	1.738	1.699	1.823	1.828	1.697	1.745	1.770	1.715	1.833	1.873	1.826	1.819	1.857	1.843	1.778	1.645	1.725	1.808	1.825	1.550	1.638	1.646	1.774	1.525	1.830	1.679	1.474	
AlIV	0.149	0.191	0.237	0.262	0.301	0.177	0.172	0.302	0.255	0.230	0.285	0.167	0.127	0.174	0.181	0.143	0.157	0.222	0.355	0.275	0.192	0.175	0.450	0.362	0.354	0.207	0.475	0.120	0.321	0.526	
Fe #	0.050	0.045	0.043	0.056	0.032	0.014	0.007	0.000	0.037	0.038	0.016	0.057	0.038	0.026	0.033	0.042	0.038	0.045	0.092	0.113	0.078	0.082	0.077	0.077	0.077	0.007	0.007	0.007	0.098		
Al VI	0.034	0.041	0.063	0.071	0.107	0.061	0.058	0.125	0.088	0.071	0.094	0.050	0.048	0.056	0.046	0.046	0.045	0.046	0.092	0.113	0.078	0.082	0.077	0.077	0.077	0.077	0.077	0.077	0.077		
Cr	0.006	0.009	0.007	0.006	0.001	0.003	0.005	0.004	0.005	0.009	0.001	0.016	0.013	0.001	0.009	0.010	0.016	0.012	0.016	0.012	0.016	0.012	0.016	0.012	0.016	0.012	0.016	0.012			
Fe #	0.047	0.074	0.087	0.084	0.087	0.063	0.071	0.071	0.071	0.071	0.071	0.071	0.071	0.071	0.071	0.071	0.071	0.071	0.071	0.071	0.071	0.071	0.071	0.071	0.071	0.071	0.071	0.071	0.071		
Fe #	0.050	0.038	0.057	0.067	0.135	0.105	0.072	0.082	0.110	0.105	0.096	0.085	0.096	0.096	0.096	0.096	0.096	0.096	0.121	0.098	0.198	0.102	0.078	0.204	0.257	0.085	0.079	0.060	0.066	0.066	
Mn ²⁺	0.813	0.792	0.743	0.717	0.638	0.787	0.777	0.664	0.711	0.723	0.690	0.758	0.797	0.767	0.768	0.776	0.655	0.633	0.705	0.657	0.617	0.582	0.654	0.665	0.751	0.758	0.564	0.415			
Mg ²⁺	0.907	0.914	0.932	0.920	0.910	0.868	0.892	0.904	0.912	0.922	0.893	0.901	0.899	0.916	0.919	0.926	0.922	0.849	0.918	0.933	0.907	0.928	0.980	0.958	0.979	0.976	0.989	0.989			
Ca ²⁺	0.022	0.021	0.026	0.032	0.025	0.047	0.018	0.021	0.033	0.025	0.024	0.029	0.023	0.014	0.013	0.017	0.023	0.020	0.026	0.027	0.035	0.033	0.032	0.030	0.030	0.029	0.028	0.027			
Na ⁺	0.000	0.001	0.001	0.000	0.001	0.000	0.000	0.000	0.001	0.000	0.001	0.000	0.000	0.000	0.000	0.000	0.000	0.001	0.001	0.001	0.001	0.001	0.001	0.001	0.001	0.001	0.001	0.001			
K ⁺	0.002	0.002	0.002	0.002	0.004	0.004	0.005	0.003	0.005	0.004	0.004	0.004	0.005	0.003	0.003	0.005	0.003	0.006	0.007	0.001	0.001	0.001	0.001	0.001	0.001	0.001	0.001	0.001			
Mn ²⁺	0.068	0.063	0.040	0.051	0.054	0.103	0.076	0.043	0.067	0.064	0.068	0.074	0.068	0.074	0.074	0.074	0.074	0.061	0.128	0.058	0.045	0.036	0.008	0.008	0.008	0.008	0.008				
Wo (%)	48.07	48.53	50.09	49.97	48.79	45.76	46.89	49.44	49.48	49.52	48.12	48.67	47.75	48.83	48.79	49.02	48.68	49.27	51.83	50.52	49.14	49.78	55.05	52.75	53.01	51.23	54.70	51.30	50.90	53.10	
En (%)	43.07	42.02	39.90	38.94	34.90	41.50	40.82	36.28	38.60	38.66	37.19	40.96	42.36	37.56	40.69	40.64	41.00	39.91	36.77	38.19	35.64	33.09	35.99	36.01	33.80	34.01	28.50	22.30			
Fs (%)	8.86	9.44	10.02	11.09	15.30	12.74	12.29	14.28	11.92	11.63	14.68	10.37	9.88	13.61	10.52	10.34	10.32	10.82	12.40	11.30	15.22	11.27	11.26	10.86	9.33	12.60	8.70	20.50	24.60		

C – core, R – rim, I – intermediate zone, M – matrix. For the complete set of analyses see Torres (1998).

TABLE 3
Representative oxide microprobe analyses of São Lameiras lavas

Geo Unit	Lithotype	Main Eruptive Formation						Serra Negra						Monte Grande - Pedra Lameira								
		Nephelinite			Basalt			Nephelinite			Nephelinite			Basalt			Nephelinite					
		Sample	116	109	124	238	682	424	367	1315	367	1315	367	1315	367	1315	367	1315	367			
		Inc	C	R	I	M	Inc	Inc	Inc	Inc	Inc	Inc	Inc	Inc	Inc	Inc	Inc	Inc	Inc			
Al ₂ O ₃ wt%	40.68	44.14	13.80	5.23	2.95	9.65	15.62	17.20	6.19	45.51	8.20	56.88	3.80	2.81	4.83	5.68	4.76	3.82	1.69	3.89	1.83	
TiO ₂	2.10	0.33	7.66	15.57	18.25	17.41	7.43	3.16	3.12	16.82	1.27	17.77	0.72	26.65	26.75	25.47	14.53	16.07	18.38	20.37	18.11	20.43
Cr ₂ O ₃	13.42	19.92	15.70	4.62	1.85	2.23	24.01	31.21	32.08	6.04	12.86	4.47	1.07	0.00	0.00	0.00	3.35	1.06	1.55	0.06	1.40	0.07
V ₂ O ₃	0.11	0.09	0.26	0.35	0.40	0.42	0.25	0.17	0.18	0.51	0.16	0.54	0.06	0.45	0.20	0.74	0.32	0.31	0.42	0.43	0.39	0.45
Fe ₂ O ₃	11.11	5.56	25.40	30.66	31.41	31.60	21.11	15.80	15.32	23.93	7.59	21.67	10.28	13.35	13.95	14.53	31.52	32.68	29.92	29.41	30.37	29.31
FeO	16.22	10.92	27.04	35.54	38.60	37.81	30.05	24.22	19.38	41.00	16.86	41.70	11.98	53.56	53.66	51.52	37.56	37.87	39.30	41.54	37.97	41.13
MnO	0.17	0.39	0.50	0.58	0.71	0.61	0.38	0.30	0.25	0.50	0.29	0.73	0.18	0.67	0.75	0.64	0.69	0.76	0.89	1.10	0.81	1.00
MgO	15.40	18.15	8.37	6.57	5.89	5.86	6.00	7.92	11.36	3.92	15.01	4.16	19.29	1.45	1.14	2.21	4.37	5.04	5.58	4.84	6.18	5.23
Total	99.21	99.50	98.74	99.13	99.69	98.90	98.89	98.40	98.90	98.91	99.55	99.24	10.46	99.94	99.26	99.95	98.03	98.56	99.44	99.11	99.43	
Al ³⁺	10933	11.475	4.371	1.744	0.864	1.002	31.158	4.921	5.232	2.092	11.995	2.729	13.974	1.304	0.978	1.641	1.943	1.620	1.281	0.578	1.307	0.624
Ti ⁴⁺	0360	0.056	1.549	3.310	3.929	3.772	1.552	0.635	0.606	3.628	0.213	3.773	0.113	5.833	5.938	5.519	3.168	3.487	3.933	4.443	3.885	4.441
Cr ³⁺	2420	3.475	3.336	1.033	0.418	0.507	52.271	6.594	6.544	1.370	22.75	0.997	0.176	0.001	0.000	0.000	0.769	0.241	0.350	0.015	0.315	0.015
V ³⁺	0.021	0.015	0.057	0.079	0.093	0.098	0.057	0.037	0.037	0.118	0.028	0.123	0.010	0.106	0.047	0.171	0.073	0.072	0.096	0.088	0.103	
Fe ³⁺	1.906	0.923	5.138	6.523	6.766	6.850	4.411	3.177	2.975	5.163	1.277	4.905	1.613	2.924	3.099	3.150	6.878	7.094	6.407	6.422	6.520	6.375
Fe ²⁺	3.092	2.015	6.079	8.404	9.240	9.108	6.978	5.412	4.182	9.832	3.153	9.847	2.088	13.037	13.249	12.412	9.110	9.135	9.352	10.080	9.060	9.942
Mn ²⁺	0.033	0.072	0.115	0.139	0.173	0.148	0.090	0.069	0.054	0.122	0.055	0.175	0.032	0.164	0.186	0.156	0.170	0.185	0.215	0.269	0.195	0.244
Mg ²⁺	5.235	5.968	3.366	2.768	2.515	2.484	3.154	4.370	5.005	1.751	5.993	0.631	0.503	0.950	1.889	2.167	2.366	2.086	2.630	2.255		
mol Usp	0.262	0.106	0.376	0.538	0.464	0.453	0.413	0.286	0.290	0.384	0.250	0.621	0.123	0.798	0.791	0.775	0.452	0.441	0.490	0.517	0.471	0.514

C – core, R – rim, I – intermediate zone, M – matrix, Inc – inclusion in olivine, Cr-sp – chromian spinel; Chr – chromites; Magn – Ti – magnetites. For the complete set of analyses see TORRES (1998).

TABLE 4
Representative plagioclase microprobe analyses of Sal Island basalts

GeoUnit	Sample	Main Eruptive F.			Serra Negra			Ponta do Altar Baixa			Monte Grande Pedra - Lume												
		115	C	M	109	M	M	1025	C	I	R	M	1001	C	I	R	M	682					
SiO ₂ wt%	53.39	57.73	51.30	52.97	51.65	51.70	61.04	51.57	50.07	49.90	52.88	49.01	54.98	49.60	49.73	51.23	51.25	48.81	48.81	49.47			
Al ₂ O ₃	29.43	23.06	29.48	28.52	28.58	29.46	23.42	29.57	30.80	31.07	29.09	29.82	27.74	31.22	30.92	30.03	30.05	31.56	31.23	29.70	31.66	31.62	31.03
TiO ₂	0.19	0.15	0.17	0.21	0.20	0.19	0.16	0.21	0.11	0.07	0.12	0.13	0.15	0.13	0.12	0.17	0.14	0.13	0.15	0.13	0.13	0.15	
Fe ₂ O ₃	0.97	0.60	0.87	0.75	1.00	0.90	0.34	0.82	0.48	0.58	0.41	0.60	0.42	0.57	0.64	0.66	0.73	0.59	0.59	0.47	0.52	0.53	0.62
MgO	0.06	0.66	0.39	0.09	0.13	0.09	0.32	0.04	0.08	0.07	0.06	0.06	0.02	0.13	0.24	0.13	0.11	0.12	0.08	0.08	0.08	0.08	0.08
MnO	0.00	0.00	0.02	0.02	0.03	0.00	0.01	0.00	0.00	0.00	0.00	0.00	0.01	0.00	0.00	0.00	0.01	0.05	0.01	0.04	0.03	0.01	0.02
BaO	0.09	2.22	0.01	0.11	0.06	0.11	0.62	0.09	0.01	0.19	0.13	0.02	0.15	0.08	0.13	0.03	0.16	0.05	0.14	0.08	0.10	0.01	0.07
CaO	11.90	4.13	11.44	12.54	12.60	5.06	12.64	13.89	14.32	11.28	13.73	9.78	14.45	14.33	12.87	13.49	14.71	15.02	12.42	16.28	15.33	14.74	14.74
Na ₂ O	3.75	3.61	3.81	4.37	3.86	3.79	6.90	3.73	3.18	2.81	4.44	3.11	5.30	2.81	2.82	3.59	3.50	2.71	2.76	3.86	2.62	2.61	2.93
K ₂ O	0.37	7.51	0.58	0.48	0.49	0.37	1.83	0.26	0.17	0.17	0.34	0.24	0.52	0.23	0.22	0.31	0.33	0.23	0.19	0.38	0.24	0.23	0.26
Total	100.15	99.68	98.30	98.96	98.73	99.25	99.68	98.95	98.80	99.17	98.74	96.72	99.06	99.24	99.14	99.02	99.77	99.19	99.23	99.19	99.47	99.36	99.38
Ca ²⁺	2.305	0.825	2.311	2.247	2.480	2.477	0.974	2.490	2.744	2.823	2.215	2.775	1.907	2.851	2.829	2.532	2.644	2.906	2.972	2.436	3.017	3.028	2.910
Si ⁴⁺	9.666	10.760	9.483	9.713	9.570	9.485	10.867	9.478	9.235	9.186	9.684	9.249	10.013	9.131	9.165	9.410	9.374	9.045	9.064	9.532	8.936	9.000	9.113
Al ³⁺	6.273	5.064	6.423	6.163	6.216	6.372	4.950	6.405	6.695	6.740	6.285	6.632	5.954	6.773	6.715	6.501	6.477	6.859	6.795	6.409	6.877	6.871	6.738
Ti ⁴⁺	0.026	0.020	0.023	0.029	0.027	0.026	0.021	0.030	0.015	0.010	0.016	0.018	0.020	0.017	0.016	0.023	0.019	0.018	0.017	0.020	0.019	0.018	0.021
Fe ²⁺	0.130	0.084	0.120	0.104	0.138	0.124	0.046	0.113	0.057	0.080	0.057	0.085	0.057	0.079	0.088	0.090	0.100	0.081	0.082	0.064	0.072	0.073	0.085
Mg ²⁺	0.017	0.185	0.107	0.025	0.037	0.026	0.087	0.012	0.023	0.020	0.016	0.017	0.004	0.036	0.036	0.031	0.034	0.022	0.010	0.021	0.025	0.025	0.025
Mn ²⁺	0.000	0.000	0.003	0.003	0.005	0.005	0.001	0.002	0.000	0.000	0.000	0.000	0.002	0.000	0.000	0.001	0.008	0.001	0.006	0.004	0.001	0.003	0.003
Ba ²⁺	0.007	0.162	0.001	0.008	0.005	0.008	0.044	0.006	0.001	0.013	0.009	0.002	0.010	0.005	0.009	0.002	0.012	0.004	0.010	0.005	0.007	0.001	0.005
Ca ²⁺	2.305	0.825	2.311	2.247	2.480	2.477	0.974	2.460	2.744	2.823	2.215	2.775	1.907	2.851	2.829	2.532	2.644	2.906	2.972	2.436	3.017	3.028	2.910
Na ⁺	1.316	1.305	1.366	1.554	1.381	1.350	2.402	1.330	1.138	1.004	1.577	1.139	1.872	1.004	1.007	1.278	1.241	0.968	0.988	1.371	0.938	0.934	1.047
K ⁺	0.086	1.787	0.136	0.113	0.114	0.096	0.420	0.062	0.041	0.040	0.080	0.058	0.120	0.054	0.052	0.073	0.076	0.054	0.045	0.059	0.056	0.055	0.061
%An	62.24	23.68	61.70	57.60	62.68	63.46	27.03	64.17	70.10	72.90	57.24	69.97	48.84	73.10	73.04	65.48	66.82	74.18	74.17	62.58	75.23	75.52	72.52
%Ab	35.27	30.61	34.81	39.34	34.35	34.16	61.15	34.08	28.83	25.75	40.46	28.54	47.83	25.40	25.41	32.69	30.98	24.36	24.46	35.00	23.20	23.10	25.84
%Or	2.49	45.71	3.49	3.06	2.95	2.88	11.82	1.75	1.07	1.36	2.30	1.49	3.33	1.51	1.55	1.98	2.19	1.46	1.37	2.42	1.57	1.38	1.64

C – core, R – rim, I – intermediate zone, M – microite in groundmass. For the complete set of analyses see TORRES (1998).

TABLE 5
Representative nepheline and melilite microprobe analyses of Sal nephelinites

Geol Unit	Main Eruptive Form.	P. Altar Baleia	M.Gr.-P. Lume	Geol Unit	P. Altar Baleia	M.Grande - Pedra Lume									
Sample	116	424	1315	Sample	424	1315	1248								
SiO ₂ (wt%)	41.37	40.89	40.04	41.08	41.14	40.89	41.34	SiO ₂ (wt %)	41.89	42.71	41.98	42.01	42.84	42.56	42.94
TiO ₂	0.06	0.08	0.08	0.09	0.12	0.11	0.10	TiO ₂	0.19	0.08	0.06	0.12	0.08	0.07	0.06
Al ₂ O ₃	33.10	33.08	32.88	33.00	32.65	32.49	32.88	Al ₂ O ₃	6.82	6.65	6.31	7.15	6.79	6.79	6.56
Fe ₂ O ₃	0.84	1.03	1.02	1.07	0.92	1.01	1.01	FeO	3.11	3.35	3.27	3.51	3.11	3.07	3.47
MnO					0.01	0.03	0.02	MnO	0.15	0.06	0.09	0.04	0.05	0.08	0.11
MgO	0.17	0.16	0.16	0.15	0.19	0.15	0.17	MgO	8.13	7.58	7.76	7.29	8.01	8.05	7.46
CaO	0.77	0.81	2.82	0.34	0.33	0.47	0.50	CaO	34.26	33.81	34.28	33.29	34.50	34.38	34.18
Na ₂ O	15.19	14.35	14.16	13.76	13.36	14.31	14.14	Na ₂ O	2.84	3.17	2.90	3.19	3.03	3.14	3.32
K ₂ O	7.57	7.72	7.25	9.84	9.83	8.51	8.31	K ₂ O	0.15	0.16	0.14	0.12	0.08	0.10	0.08
BaO	0.21	0.42	0.38	0.67	0.52	0.75	0.49	BaO	0.13	0.60	0.52	0.55			
Total	99.27	98.52	98.79	99.99	99.07	98.72	98.95	Total	97.67	98.17	97.32	97.27	98.49	98.24	98.18
Si ⁺⁴	8.122	8.095	7.946	8.099	8.162	8.135	8.161	Si ⁺⁴	3.895	3.958	3.933	3.928	3.937	3.924	3.965
Ti ⁺⁴	0.009	0.012	0.012	0.013	0.018	0.016	0.015	Ti ⁺⁴	0.013	0.006	0.004	0.008	0.006	0.005	0.004
Al ⁺³	7.659	7.720	7.691	7.669	7.634	7.616	7.650	Al ⁺³	0.747	0.726	0.697	0.788	0.735	0.738	0.714
Fe ⁺³	0.123	0.153	0.153	0.158	0.138	0.151	0.150	Fe ⁺²	0.241	0.260	0.256	0.275	0.239	0.237	0.268
Mn ⁺²					0.001	0.006	0.003	Mn ⁺²	0.012	0.005	0.007	0.003	0.004	0.006	0.009
Mg ⁺²	0.050	0.046	0.048	0.043	0.058	0.043	0.050	Mg ⁺²	1.127	1.047	1.084	1.016	1.097	1.107	1.027
Ca ⁺²	0.161	0.171	0.600	0.072	0.070	0.100	0.106	Ca ⁺²	3.413	3.357	3.441	3.335	3.397	3.396	3.381
Na ⁺¹	5.783	5.507	5.450	5.261	5.139	5.519	5.412	Na ⁺¹	0.513	0.569	0.526	0.578	0.540	0.561	0.594
K ⁺¹	1.895	1.949	1.835	2.474	2.488	2.160	2.092	K ⁺¹	0.017	0.019	0.017	0.014	0.009	0.012	0.009
Ba ⁺²	0.016	0.033	0.029	0.052	0.041	0.059	0.038	Ba ⁺²	0.005	0.022	0.019	0.020			
% Ne	72.8	70.6	72.4	64.9	63.6	68.7	68.3	% Aker	66.5	66.0	67.5	63.9	66.3	66.3	66.0
% Ks	26.6	27.8	27.6	34.0	34.3	29.9	29.4	% Gehl	33.5	34.0	32.5	36.1	33.7	33.7	34.0
% Qz	0.6	1.6	0.0	1.1	2.1	1.3	2.4								

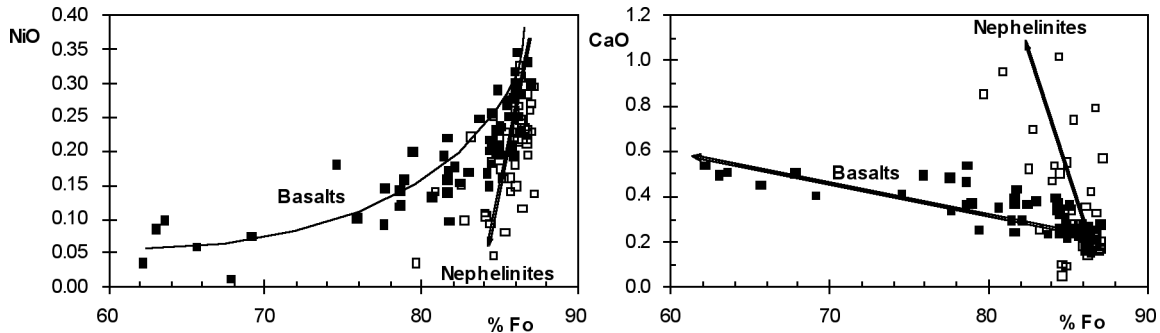


Fig. 4 – NiO and CaO (wt %) vs. Fo diagrams for olivine in Sal basaltic (filled squares) and nephelinitic (open squares) lavas.

nephelinites (Ca > 0.94 a.f.u.) pointing out to a greater importance of non-quadrilateral substitutions in nephelinites.

Pyroxene chemistry indicates that the S4 type ($\text{CaMg}_{0.5}\text{Ti}_{0.5}\text{Al}^{\text{IV}}\text{SiO}_6$) is the most important non-quadrilateral substitution in the Sal pyroxenes (see Fig. 5).

Sub-solidus esseneites, given their low Ti and Cr, and high Fe³⁺ relatively to Al in M1 position, are dominated by FATS (Fe³⁺-Al Tschermark or esseneite) component substitution (Fig. 5).

Oxides are predominantly members of the magnetite-ulvöspinel solid solution series. Ti-magnetites

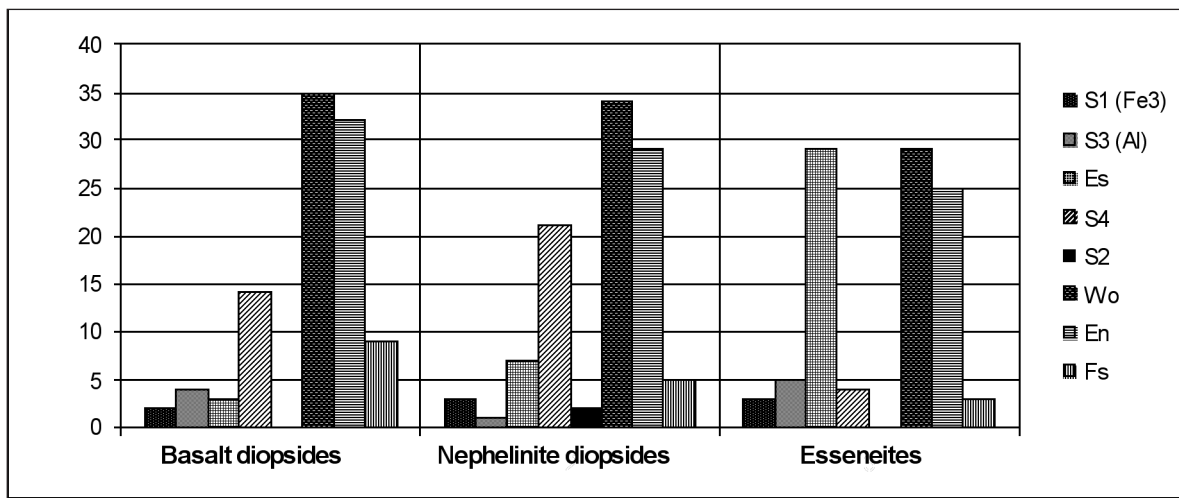


Fig. 5 – Histograms of relative percentages of the various types of substitution in pyroxenes (MORIMOTO *et al.* 1988) from basaltic and nephelinitic rocks.

TABLE 6
Representative perowskite microprobe analyses of Sal lavas

Geol Unit	Main E. F.	Ponta do Altar Baleia			Mte. Grande - Pedra Lume		
Lithotype	Neph	Nephelinite			Nephelinite		
Sample	116	424			1315	1247	1248
TiO ₂ (wt %)	55.49	55.14	55.55	56.03	56.07	55.24	55.91
Al ₂ O ₃	0.17	0.67	0.48	0.21	0.26	0.23	0.20
Cr ₂ O ₃	0.08			0.05			
FeO	0.94	1.36	1.62	1.06	1.04	1.35	1.06
MnO	0.01		0.01		0.05	0.08	0.01
MgO	0.04	0.16	0.10	0.04	0.03	0.03	0.04
CaO	37.83	38.36	39.19	38.73	37.81	39.33	38.25
Na ₂ O	0.44	0.44	0.22	0.20	0.36	0.35	0.24
K ₂ O	0.02	0.08	0.06	0.01	0.04	0.01	0.01
Total	95.02	96.21	97.22	96.32	95.65	96.62	95.72
Ti ⁺⁴	7.9691	7.8320	7.8241	7.9411	7.9916	7.837	7.969
Al ⁺³	0.0382	0.1490	0.1065	0.0476	0.0576	0.051	0.045
Cr ⁺³	0.0114			0.0079			
Fe ⁺²	0.1507	0.2150	0.2534	0.1663	0.1646	0.213	0.168
Mn ⁺²	0.0021		0.0010		0.0082	0.013	0.002
Mg ⁺²	0.0118	0.0450	0.0282	0.0106	0.0096	0.008	0.011
Ca ⁺²	7.7396	7.7630	7.8631	7.8202	7.6779	7.95	7.768
Na ⁺¹	0.1611	0.1600	0.0783	0.0716	0.1318	0.128	0.088
K ⁺¹	0.0051	0.0200	0.0144	0.0032	0.0085	0.002	0.002

TABLE 7
Major and trace element analyses of Sal Island lavas

Sample	Main Eruptive Formation				Ponta Alta Batalha Complex				Serra Negra				Monte Grande - Pedra Lume					
	115	475	116	103	1465	1001	678	424	13	1025	108	682	977	1315	238	367	192	
Rock Type					Basalt	Neph_m	Neph_m	Melilite	Basalt	Neph_m	Melilite	Basalt	Melilite	Melilite	M_neph	M_neph		
SO ₂ (wt%)	42.89	39.46	38.64	38.43	45.24	41.54	39.90	38.97	34.47	45.71	45.21	42.39	43.25	36.83	34.85	39.78	39.08	
TiO ₂	3.62	4.48	2.78	3.85	2.56	2.79	2.95	3.43	4.08	3.17	3.40	3.73	2.81	3.36	3.74	3.89	3.36	
Al ₂ O ₃	16.05	13.75	11.55	10.59	13.57	13.03	13.96	9.92	10.63	12.97	12.94	12.63	12.96	11.19	10.89	12.09	11.33	
Fe ₂ O ₃	5.37	6.57	4.66	5.24	2.20	4.50	8.12	4.71	6.31	4.75	4.70	4.70	3.28	5.72	6.34	4.91	5.29	
FeO	5.98	7.34	7.83	7.53	9.79	8.17	5.29	7.46	5.92	7.10	6.33	7.66	8.75	6.24	5.92	6.69	5.92	
MnO	0.23	0.22	0.18	0.20	0.18	0.18	0.25	0.20	0.23	0.17	0.18	0.19	0.21	0.22	0.21	0.18	0.19	
MgO	6.45	7.51	12.74	14.49	10.61	12.16	9.85	16.40	13.25	10.70	10.50	10.81	12.97	13.01	12.25	14.61	14.66	
CaO	12.90	12.42	12.54	14.41	11.50	11.33	12.73	13.48	16.27	10.57	11.48	11.66	11.95	16.08	15.98	13.12	12.79	
Na ₂ O	1.98	2.70	4.28	2.37	2.07	2.47	1.65	2.50	3.50	1.93	1.84	2.54	1.98	2.64	3.54	3.41	2.88	
K ₂ O	1.17	0.98	1.39	0.74	0.83	0.97	0.89	1.29	0.98	0.75	1.22	1.19	1.30	0.48	1.18	1.23	0.78	
P ₂ O ₅	0.66	0.54	0.76	0.86	0.37	0.45	0.31	0.82	1.69	0.35	0.49	0.48	0.44	1.68	1.65	1.01	0.93	
H ₂ O										3.55								
LOI	4.00	1.66	1.30	1.08	2.41	0.80	0.82	2.98	1.83	1.72	2.03	1.00	2.60	2.66	1.42	2.86	5.20	
Total	97.31	99.98	100.01	100.01	100.00	100.25	100.00	100.00	100.00	100.01	100.00	99.99	100.00	99.98	100.01	100.01	100.00	
Mg #	51.51	50.25	63.38	67.83	61.63	63.94	58.22	71.41	67.13	62.64	63.93	61.84	64.78	66.99	66.60	66.28	70.91	70.37
Cr(ppm)	50	84	428	487	181	331	169	650	146	399	381	319	376	216	237	304	359	
Ni	97	52	352	385	183	199	156	555	303	292	251	251	285	277	277	265	288	
Sc	22	19	22	24	15	26	21	25	22	24	25	24	26	23	25	24	27	
Cu	122	28	63	133	118	49	163	127	95	127	104	54	117	129	70	79	49	
Zn	110	93	95	96	103	97	99	96	101	128	100	90	98	88	101	86	74	
Rb	27	21	18	24	13	17	27	35	18	16	27	18	27	22	34	15	20	
Cs	0.21	0.42	0.41	0.20	0.20	0.20	0.20	0.21	0.20	0.20	0.20	0.20	0.20	0.21	0.41	0.61	0.53	
Ba	423	583	689	158	340	389	559	1082	278	385	428	341	752	1002	599	749	598	
Sr	954	694	1010	1099	521	488	624	1030	1888	511	593	535	596	1497	1457	991	896	
Ta	2.77	4.06	3.15	3.14	1.62	2.66	3.02	4.03	4.74	1.94	2.85	2.86	2.73	4.00	5.03	4.26	3.19	
Nb	39.1	57.3	59.0	45.6	31.3	42.0	37.5	51.4	96.9	275	326	42.9	36.4	61.6	85.3	54.8	60.7	
Hf	4.32	4.68	4.47	5.27	2.53	4.51	5.21	5.34	5.87	428	529	531	465	503	6.37	5.78	4.94	
Zr	224	196	236	250	189	181	248	250	376	199	237	218	224	321	329	305	270	
Y	26	25	24	24	18	17	24	24	46	19	22	22	22	29	37	23	22	
Th	290	5.10	5.50	1.00	1.80	2.00	5.00	10.10	1.90	2.10	1.90	1.80	8.00	10.00	4.40	5.40	3.30	
U	0.82	0.83	1.32	0.40	0.82	0.73	1.21	3.09	0.41	0.41	0.41	0.71	2.05	2.77	1.22	1.34	1.48	
La	39.3	37.7	57.4	57.3	13.8	24.1	28.3	59.3	116.0	21.1	25.5	24.9	25.5	88.8	109.0	51.5	63.5	
Ce	79	77	102	103	29	50	60	115	201	44	54	54	52	157	197	94	116	
Nd	37	36	43	47	15	28	30	51	79	22	31	28	26	65	77	44	51	
Sm	7.32	7.32	8.24	8.58	3.14	5.66	6.55	9.77	14.60	5.36	6.63	6.54	5.74	12.40	14.50	8.67	9.39	
Eu	2.25	2.37	2.73	2.97	1.20	2.00	2.26	3.25	4.60	1.84	2.28	2.12	1.98	3.83	4.57	2.79	3.00	
Tb	1.00	1.00	1.20	0.60	0.90	1.00	1.20	1.70	0.80	0.90	1.00	0.80	1.50	1.70	1.20	1.10	1.00	
Yb	2.03	1.90	1.46	1.47	1.12	2.22	1.66	2.29	1.56	1.76	1.68	1.66	2.01	2.53	1.87	1.71	1.70	
Lu	0.26	0.26	0.18	0.20	0.14	0.22	0.27	0.21	0.19	0.22	0.21	0.21	0.27	0.30	0.25	0.23	0.22	

Neph_m – nepheline with melilite; M_neph – melanepheline. For the complete set of analyses see TORRES (1998).

TABLE 8
Sr and Nd isotopic analyses of Sal Island lavas

Geol. Unit	Sample	Rock type	$^{87}\text{Sr}/^{86}\text{Sr}$	$^{143}\text{Nd}/^{144}\text{Nd}$	εNd
MEF	115	Basalt	0.703350 ± 10	0.513029 ± 22	7.63
	475	Basalt	0.703460 ± 10		
	116	Neph mel	0.703200 ± 10	0.512802 ± 33	3.20
	103	Neph mel	0.703080 ± 8	0.512888 ± 31	4.88
PAB	1465	Basalt	0.703220 ± 8		
	1001	Basalt	0.703380 ± 10	0.512774 ± 26	2.65
	679	Basalt	0.703370 ± 6	0.512771 ± 30	2.59
	676	Neph mel	0.703230 ± 7		
	424	Melilitite	0.703390 ± 14	0.512927 ± 25	5.64
SN	13	Basalt	0.703390 ± 7		
	1025	Basalt	0.703380 ± 6	0.512770 ± 56	2.57
	109	Basalt	0.703380 ± 6	0.513000 ± 24	7.06
MGPL	682	Basalt	0.703210 ± 10	0.512885 ± 29	4.82
	197	Melilitite	0.703230 ± 9	0.513027 ± 34	7.59
	1315	Melilitite	0.703130 ± 10	0.512900 ± 24	5.11
	238	Melaneph	0.703670 ± 9	0.512971 ± 22	6.50
	367	Melaneph	0.703580 ± 7	0.512981 ± 26	6.69
	192	Melaneph	0.704101 ± 10	0.513118 ± 25	9.36

MEF – Main Eruptive Formation, PAB– Ponta do Altar Baleia Complex SN – Serra Negra Formation, MGPL – Monte Grande – Pedra Lume.

($\text{TiO}_2 = 14.53 - 26.75 \text{ wt } \%$) display progressive substitution of Cr + Al (0.59 – 7.71 a.f.u.) by Ti, Fe^{3+} and Fe^{2+} (% mol Usp = 43 – 80) with the advance of magmatic evolution. A few Al-rich chromian spinels and chromites (in particular those included in olivine phenocryst cores) can be considered as earlier crystallization phases that fractionated under relatively high-pressure conditions (e.g. MATA & MUNHÁ, 2004). Their composition ranges within the spinel-magnesiochromite solid solution due to $\text{Cr} \leftrightarrow \text{Al}$ exchange.

Plagioclase phenocrysts range from bytownite (An_{73}) cores to labradorite (An_{57}) rims. Groundmass microlites are highly variable extending from compositions similar to those characterizing phenocrysts down to 24 mol % An, reflecting progressive anortite ($\text{CaAl}_2\text{Si}_2\text{O}_8$) replacement by albite ($\text{NaAlSi}_3\text{O}_8$) along the fractionation processes.

Nepheline contains up to 9.8 wt % K_2O corresponding to 34 mol % Ks.

Melilitite ranges from 64 to 67 mol % of akermanite.

Perowskite quantitative analyses show considerable substitutions of Ca by rare earth elements (knopite) that

were analyzed only qualitatively. Moreover, there is evidence for the Nb and small amounts of Ta replacing Ti (dysanalyte and loparite).

6 – GEOCHEMISTRY

6.1 Major and trace-element results

The studied Sal volcanic rocks (see Table 7 for major and trace-element analysis results) have low silica contents ($\text{SiO}_2 \approx 34$ to $\approx 46 \text{ wt } \%$) and high alkalis concentrations (Na_2O up to 4.73%; K_2O up to 2.6%), plotting within the alkalic field on the TAS (total alkalis vs. SiO_2) diagram – Fig. 6 (LE BAS *et al.*, 1986, LE MAITRE, 2002). $\text{Na}_2\text{O}/\text{K}_2\text{O}$ (wt %) in excess of 1 ($\bar{x} = 2.36 \% \pm 0.09$), allows to consider these lavas as sodic following the proposal of Middlemost (1975).

CIPW normative compositions range from *Ne* normative (1 – 20 %) to *Hy* normative (3 – 17 %), with the great majority of samples (88%) being silica undersaturated and with a considerable number (45%) of them corresponding to foidites (Fig. 6 and 7).

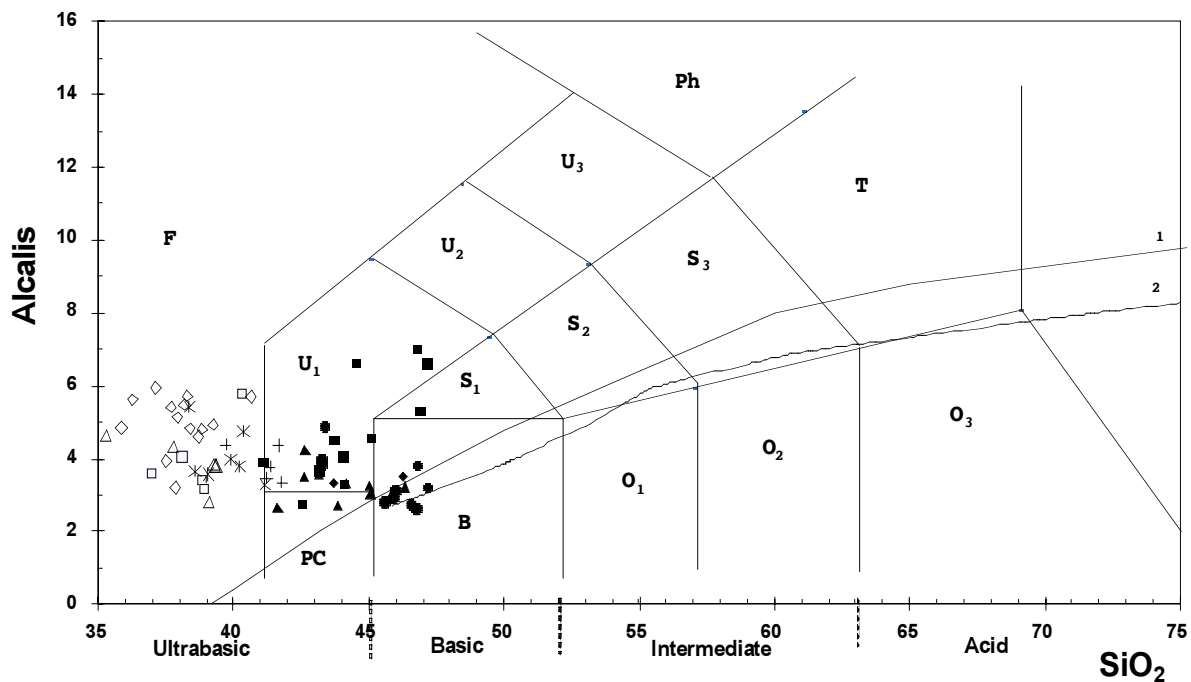


Fig. 6 – Silica – Alcalis (TAS) diagram (LE BAS *et al.*, 1986). Lines 1 and 2 according to IRVINE AND BARAGAR (1971) and KUNO (1966). Open symbols – nephelinites and melilitites. Filled symbols – basalts and basanites. Squares – Main Eruptive Formation, circles – Serra Negra Eruptive Formation, triangles – Ponta do Altar-Baleia Complex, diamonds (melilitites and melilite nephelinites) and asterisks (nephelinites) from Monte Grande Pedra Lume Formation.

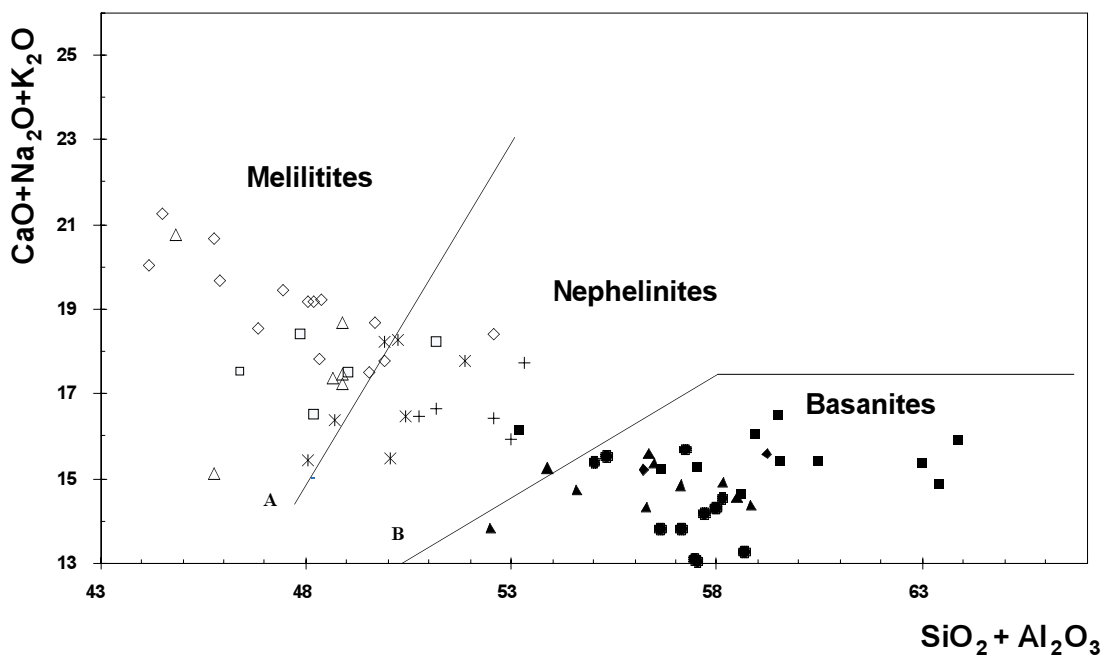


Fig. 7 – Discrimination diagram for melilititic, nefelinitic and basanitic rocks, according to LE BAS (1989). Symbols as in previous figure.

All the hyperstene normative samples (12 % of the analysed samples) belong to the Serra Negra Eruptive Formation and are also characterized by distinct trace element ratios (e.g. \bar{x} Y/Nb = 0.60 ± 0.02; $\bar{x}(\text{La}/\text{Sm})_n$ = 2.49 ± 0.03; $\bar{x}(\text{La}/\text{Yb})_n$ = 10.24 ± 0.39) when compared to those ratios of undersaturated lavas from younger and older formations $\bar{x}Y/\text{Nb}$ = 0.49 ± 0.08; $\bar{x}(\text{La}/\text{Sm})_n$ = 3.79 ± 0.71; $\bar{x}(\text{La}/\text{Yb})_n$ = 20.65 ± 8.58). The majority of Serra Negra lavas plot in the basalt field of the TAS diagram (Fig. 6) occupying a position close to the KUNO (1966) and IRVINE AND BARAGAR (1971) compositional dividers between alkaline and tholeiitic suites, but clearly inside the alkali basalt field defined by BELLINI *et al.* (1983; in: LE MAITRE *et al.*, 2002).

The studied lavas are strongly enriched in incompatible elements with La being 50 to 500 times more concentrated than in chondrites. As seen in Fig. 8, REE are significantly fractionated, with $(\text{La}/\text{Yb})_n$ ranging from 8.84 to 36.34. This fractionation is inversely correlated with the degree of silica-undersaturation or silica content, increasing from alkali basalts to melilitites through basanites and nephelinites (Fig. 9).

Other incompatible trace elements concentrations also vary within a significant range and show an increase with both differentiation and degree of silica undersaturation. Sal mafic lavas present extended trace element patterns with the relative degree of enrichment for the different elements tentatively reflecting the order of incompatibility usually determined for magma genesis processes of non-orogenic oceanic lavas. This is demonstrated, for example, by values of Zr/Y (4.19 to 13.72; \bar{x} = 10.21 ± 0.22), Nb/Zr (0.14 to 0.60; \bar{x} = 0.21 ± 0.01), and Ba/Sr (0.30 to 1.55; \bar{x} = 0.79 ± 0.04) higher than those reported for chondrites (McDONOUGH & SUN, 1995). However, a significant difference arises from the patterns depicted by melilitic/nephelinitic rocks as compared with those of basalts (Fig. 10). Contrasting with basalts, strongly undersaturated rocks are characterized by marked Rb, K, and Hf negative anomalies.

6.2 Sr and Nd Isotopic results

The obtained results (see Table 8) are somewhat variable, covering the following ranges: $^{87}\text{Sr}/^{86}\text{Sr}$ =

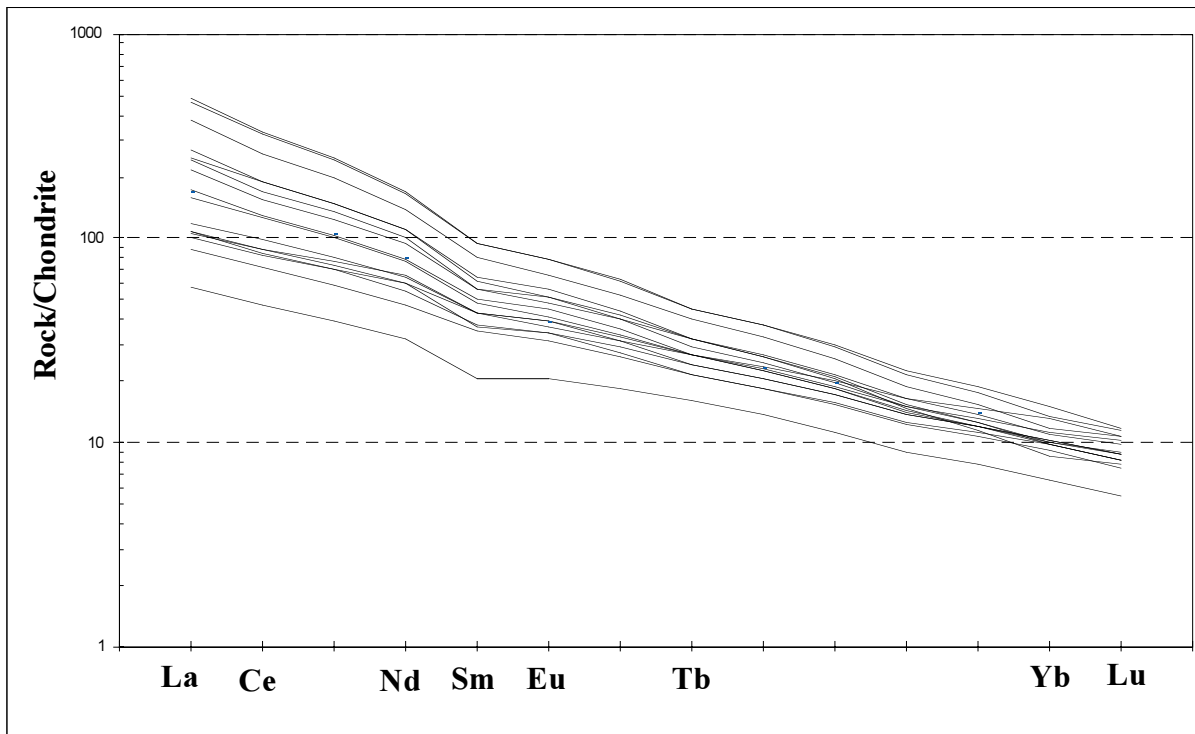


Fig. 8 – Chondrite normalized (MCDONOUGH AND SUN, 1995) Rare Earth Elements pattern for studied lavas from Sal Island.

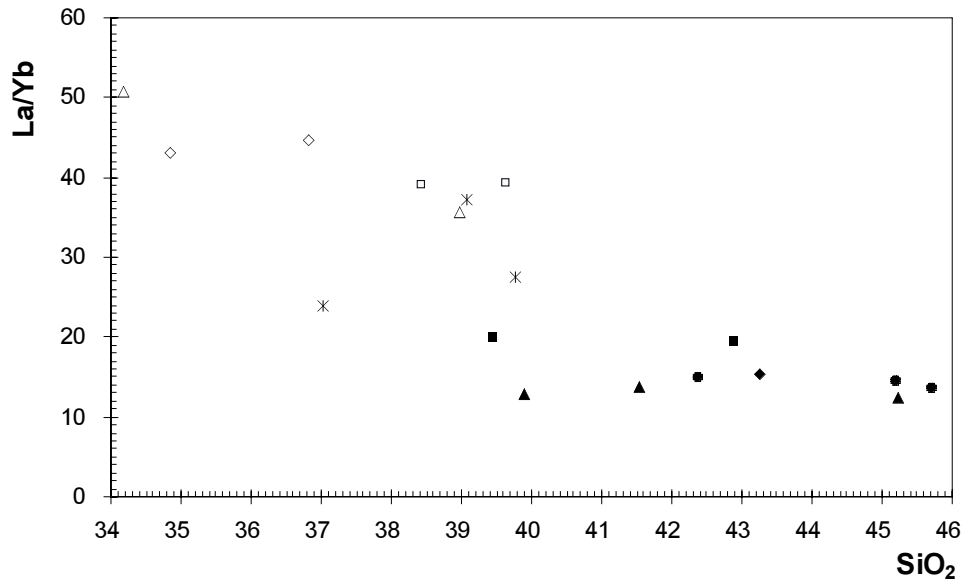


Fig. 9 – La/Yb vs. SiO_2 diagram. Open symbols – Basanites, nephelinites and melilitites. Filled symbols – Basalts. Squares – Main Eruptive Formation, circles – Serra Negra Eruptive Formation, triangles – Ponta do Altar-Baleia Complex, diamonds (melilitites and melilite-nephelinites) and asterisks (nephelinites) from Monte Grande Pedra Lume Formation.

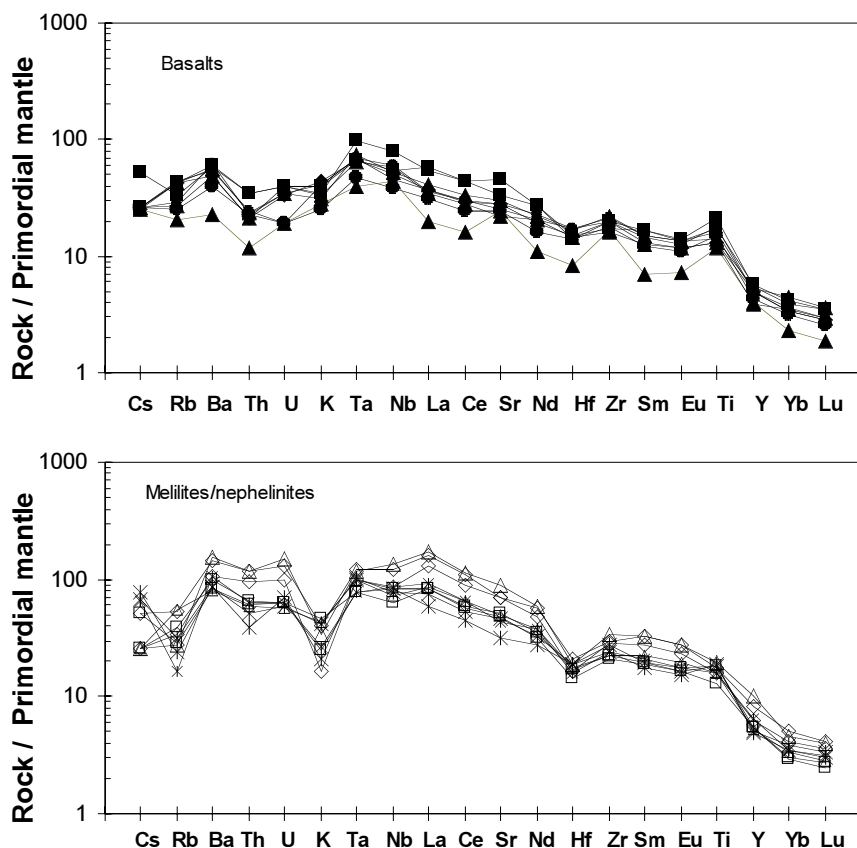


Fig. 10 – Primitive mantle-normalized (SUN & McDONOUGH, 1989) incompatible element diagrams for basaltic and melilititic/nephelinitic rocks. Symbols as in previous figure.

$= 0.703080 - 0.704101$ and $^{143}\text{Nd}/^{144}\text{Nd} = 0.512770 - 0.513118$. Sr isotopic ratios tend to be negatively correlated with $^{143}\text{Nd}/^{144}\text{Nd}$, with the majority of samples plotting in the depleted quadrant ($\epsilon\text{Sr} < 0$; $\epsilon\text{Nd} > 0$) of the Sr-Nd diagram (Fig. 11). This indicates the derivation from source(s) with time-integrated Rb and Nd depletion relative to Sr and Nd, respectively. Sal lavas tend to plot below the mantle array and close to the composition of the HIMU mantle component. However, some of the analysed samples are characterized by high $^{87}\text{Sr}/^{86}\text{Sr}$, for a given $^{143}\text{Nd}/^{144}\text{Nd}$, as compared with samples from other islands of the Cape Verde archipelago. This is interpreted as reflecting the effects of alteration, which modified the magmatic Sr isotopic signatures but not the Nd ones.

It is interesting to note that some of the samples (thought unaffected by alteration processes), present $^{143}\text{Nd}/^{144}\text{Nd}$ ratios down to 0.51277, being clearly lower than those typically assigned to the HIMU and DMM mantle source components, usually considered as the main contributors for the mantle sources of the Northern Cape Verde islands.

7 – DISCUSSION

7.1 Age constraints

The Sal geochronological data (TORRES *et al.*, 2002a; HOLM *et al.*, 2008; see also this paper: 3 – Geology and Geochronology), as well those published for the other Cape Verde islands (see below) allow the discussion of some aspects of the archipelago evolution.

The most ancient volcanic rocks outcropping at the Cape Verde Archipelago have been described from the islands of Maio and Santiago, where late Jurassic basalts occur (STILLMAN *et al.*, 1982; GERLACH *et al.*, 1988). However the MORB affinities of these rocks led DE PAEPE *et al.* (1974) to consider them as representing uplifted ocean-floor (see also GERLACH *et al.*, 1988; MILLET *et al.*, 2008).

Considering the age (25.6 Ma) obtained for the Old Eruptive Complex of Sal (TORRES *et al.*, 2002a) and the published geochronological data for the Cape Verde Archipelago (GRIFFITHS *et al.*, 1975; GRUNAU *et al.*, 1975;

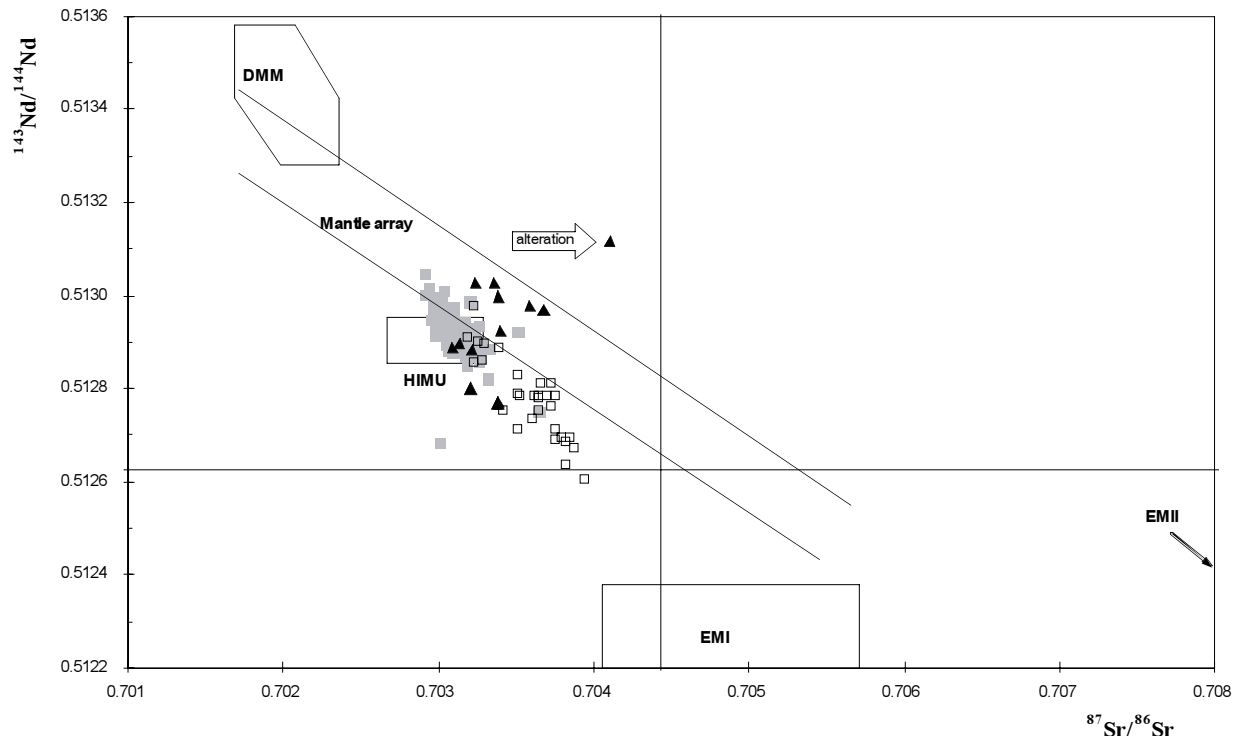


Fig. 11 – Diagram $^{143}\text{Nd}/^{144}\text{Nd}$ vs. $^{87}\text{Sr}/^{86}\text{Sr}$ for Cape Verde archipelago lavas. Mantle component fields and 'Mantle array' from ZINDLER & HART (1986). Square symbols correspond to data in literature (GERLACH *et al.*, 1988; DAVIES *et al.*, 1989; JORGENSEN & HOLM, 2002; HOLM *et al.*, 2006; MILLET *et al.*, 2008). Filled squares – Northern Islands (CVN), open squares – Southern Islands (CVS). Black triangles represent new data for Sal island.

MITCHELL *et al.*, 1983; CAHEN *et al.*, 1984; TORRES *et al.*, 2002a; PLESNER *et al.*, 2002; MADEIRA *et al.*, 2005; BOSSE *et al.*, 2007; DUPRAT *et al.*, 2007; HOLM *et al.*, 2008; DYHR & HOLM, 2010; FOEKEN *et al.*, 2009; MADEIRA *et al.*, 2010; ANCOCHEA *et al.*, 2010), we conclude that Sal preserves the most ancient emerged rocks of the Cape Verde hotspot. However, considering the evidences for K-Ar age resetting of late Jurassic basalts at 40-50 Ma, which is attributed to hotspot activity (MITCHELL *et al.*, 1983), it is suggested that the Cape Verde plume related magmatism must have started some 25 Ma before the genesis of the first emerged testimonies.

The lack of a well defined island lineament, the proximity to the West African craton and the synchronous tectonic and magmatic evolution of the islands of Maio (Cape Verde) and Fuerteventura (Canary) lead some authors (KING & RITSEMA, 2000; PATRIAT & LABAILS, 2006; KING, 2007) to argue against a mantle plume origin for the Cape Verde archipelago. Indeed, the lack of a well defined rectilinear hotspot track is, at first sight, somewhat surprising. However, it must be remembered that the north-eastward absolute motion of the African plate slowed abruptly 30 Ma ago as a consequence of its collision with Eurasia (SILVER *et al.*, 1998). According to these authors, the African plate drift in the last 10 Ma is lower than 0.8 cm yr⁻¹. If we also take into account that the rotation pole of the African Plate in the last 6 Ma (18.50°N, 17.78°W; POLLITZ, 1991) is relatively close to Cape Verde, we are compelled to accept that a long and well defined hotspot track is not expectable in the Cape Verde region, despite of the long history of volcanic activity.

It should be mentioned that (when considered as a whole) the Cape Verde islands display a very complex age distribution pattern; there is, however, a tendency for east-west age decrease. This is shown by a comparison of the ages of basal complexes of the eastern islands of Sal (25.6 Ma; TORRES *et al.*, 2002a) and Maio (21.1 Ma; GRUNAU *et al.*, 1975) with the ages of similar complexes in the western islands of the northern (Santo Antão: 7.6 Ma; PLESNER *et al.*, 2002) and southern islands (Brava: 2.90 Ma; MADEIRA *et al.*, 2010) alignments.

When considered separately, the Southern Cape Verde islands present a clear south-western age decreasing trend, which is primarily suggested by morphological criteria. In fact, Maio Island located on the northeast end of the alignment presents much more eroded landforms than the other Southern Islands (e.g. SERRALHEIRO *et al.*, 1970; MADEIRA *et al.*, 2008). On the other hand the

isotopic ages obtained for Brava (MADEIRA *et al.*, 2010), the fact that the great majority of the exposed volcanics at Fogo are younger than 130 ka (FOEKEN *et al.*, 2009), the occurrence at Fogo of more than 20 eruptions since the discovery and settlement of the island some 550 years ago (TORRES *et al.*, 1997, 1998a), and the occurrence to the southwest of Brava of the Cadamosto seamount, a seismically active 3 km tall volcanic edifice (GREVEMEYER *et al.*, 2009), suggest that we are faced with a hotspot track resulting from lithosphere migration over a fixed mantle plume, which would now be centred underneath the Fogo/Brava/Cadamosto region (e.g. TORRES *et al.*, 1998b; GREVEMEYER *et al.*, 2009). On the other hand the location of the Northern Islands has been considered as consequence of translithospheric fractures constraining the location of island buildings (TORRES *et al.*, 1998b). Large scale fault-controlled magma transport for more than 3000 km was clearly demonstrated in the Ferrar Large Igneous Province (ELLIOT *et al.*, 1999) conferring feasibility to the above mentioned hypothesis, which may imply “horizontal” magma transport of some hundred km from the upward plume batches of magmas to the local(s) of eruption.

Alternatively, HOLM *et al.* (2008) consider the plume presently centred on a region located Northwest of Sal Island, close to the places where the depth, geoid and heat flow anomalies reach its maxima. Following these authors, channelling by erosion in a swell root by different ponding batches of buoyant plume mantle would explain the spatial and age distribution of the islands. This is clearly an open question.

Notwithstanding that the Cape Verde plume is characterized by a plume flux which is only 9 to 18% of the values reported to Hawaii and Canary islands, respectively (see SCHUBERT *et al.*, 2001; HOLM *et al.*, 2008), it is significant that the Cape Verde Rise constitutes the largest reported oceanic swell (e.g. LODGE AND HELFFRICH, 2006). The above mentioned semi-stationary position of the lithosphere and a long-term magmatic history (during at least 26 Ma) explains how a weak plume produced such a prominent swell (see also MATA *et al.*, 2010).

The data obtained by TORRES *et al.* (2002a) for Sal, allow the conclusion that the outcropping volcanics cover a significant time span (\approx 26 Ma) with two important volcanic hiatus as long as \approx 3 and \approx 4 Ma. The volcanism has been inactive since 0.6 Ma ago. The same authors obtained an age 16.3 Ma for an essexitic rock considered to be part of the Old Eruptive Complex. Considering the age determined for the Main Eruptive

Formation (15.8 Ma), those plutonic rocks inside the Old Eruptive Complex can be substantially younger than the enclosing rocks, being coeval of volcanics erupted during later stages of the volcanostratigraphic evolution of the island. However, it should be emphasized that an age resetting can not be completely discarded for those essexites.

7.2 Petrogenesis

The estimated olivine saturation temperatures (basalts: 1266 to 1326°C; nephelinites: 1324 to 1363°C; see 5.2) are indicative that Cape Verde primitive magmas were hotter than the expected temperature for the asthenosphere (\approx 1280°C; e.g. MCKENZIE & BICKLE, 1988; WATSON, 1993). This allows consider that they were originated from a thermally driven mantle plume (see also PUTIRKA, 2008). This percept is endorsed by the estimated temperature of magmatic segregation calculated using the lavas major element composition and the methodology proposed by ALBARÈDE (1992), which are also above 1280°C (see below).

As depicted by the TAS diagram (Fig. 6) Sal lavas are characterized by a limited range of compositions, only basic and ultrabasic rocks being represented. Indeed, intermediate lavas are completely absent, clearly contrasting with that described for other Cape Verde islands where phonolites are volumetrically important (Brava: MOURÃO *et al.*, 2010, MADEIRA *et al.*, 2010; Boavista: DHYR & HOLM, 2010; Santo Antão: PLESNER *et al.*, 2002; HOLM *et al.*, 2006) (see also BEBIANO, 1932). This feature demonstrates that magmatic differentiation processes played a significantly less important role on the chemical variability of the erupted Sal magmas, suggesting that magma chambers were ephemeral and/or volumetrically not significant. This hypothesis is supported by the occurrence of ultramafic mantle xenoliths (see 5.1 Petrography) which indicates that magmas carrying them did not pass through a shallow subcaldera magma reservoir (e.g. CLAGUE 1988). At Sal Island intermediate rocks are only represented as minor volumetric intrusions (Old Eruptive Complex) and by some phonolitic and trachytic dykes cutting the volcanic sequence.

An insight on the genetic processes of the Sal Island magmas is offered by the study of rocks representative of “nearly primary” magmas ($Mg\# > 58$; $Ni > 150$ ppm). These highly enriched primitive lavas are characterized

by low Yb (1.12 to 2.53 ppm) and Lu (0.14 to 0.30 ppm) contents and by strong fractionation between light and heavy REE [$(La/Yb)_n = 8.84$ to 36.34], characteristics which are indicative of a source characterized by the presence of residual garnet.

The K negative anomalies portrayed by melilitic/nephelinitic rocks have been described in HIMU-type lavas and considered to reflect the K depletion of the subducting oceanic crust occurred during dehydration at subduction zones (LASSITER, 2004). However, for Sal lavas, the increase of Ce/K along with Ce (a proxy of the partial melting degree) indicates a higher compatibility for K than Ce, in opposition to that theoretically expected from melting of sources without K-bearing minerals. This is strongly suggestive that Sal magmas equilibrated with a K-rich residual phase (amphibole and/or phlogopite) capable to preferentially retain K relatively to the adjacent LILE and HFSE (see FRANCIS AND LUDDEN 1995). Considering that the degree of incompatibility of trace elements during partial melting can be inferred from the interception of regression lines in binary diagrams (HANSON, 1989) and that, for Sal $D_K \approx D_{Sr} > D_{Rb} > D_{Ba}$, amphibole is probably the dominant K-bearing residual phase (e.g. $D_K^{amph} \approx 1.0$, $D_{Rb}^{amph} \approx 0.3$; $D_K^{phlo} \approx 4.0$, $D_{Rb}^{phlo} \approx 6.0$; $D_{Rb}^{amph} \approx 6.0$, $D_{Ba}^{amph} \approx 0.5$; $D_{Ba}^{phlo} \approx 2.1$; $D_{K/Sr}^{mica/liq} \geq 10$ e $D_{Sr/Ba}^{mica/liq} \leq 0.1$; see ADAM *et al.*, 1993; LA TOURRETE *et al.*, 1995; FOLEY *et al.*, 1996; SPÄTH *et al.* 2001).

Accepting that Yb contents are roughly invariant during partial melting of a garnet-bearing mantle source (\approx two times that of chondrites; CLAGUE & FREY, 1982) estimates of melting percentages during Sal magma(s) genesis may be obtained by the inverse approach of MINSTER & ALLÈGRE (1978). This approach substantiates low, but variable, degrees of partial melting, from 1.2 to 4.8 % for melilitic/nephelinite magmas to 6.1 to 8.8 % for basaltic magmas (in agreement with experimental data obtained for melting of garnet lherzolite lithologies; e.g. GUDFINNSSON & PRESNALL, 2005).

Considering that garnet is stable in mantle peridotites at depths in excess of 60 km, the thickness of the Cape Verde lithosphere (\approx 83 km; CAZENAVE *et al.*, 1988) and the large abundance of rocks presumably generated by very low degrees of partial melting, we consider that Sal magmas were generated by adiabatic melting of the ascending mantle plume, with the thick lithosphere lid limiting the minimum depth of melting and, consequently, also the amount of magma generated (see WATSON & MCKENZIE, 1991). However, it should be

emphasized that amphibole is not stable at temperatures above 1150°C (e.g. WALLACE & GREEN, 1991), i.e., at temperatures prevailing in the asthenosphere or in mantle plumes. Thus, the evidence (presented above) for equilibration of the most undersaturated Sal magmas with amphibole implies the interaction of plume magmas with the lithospheric mantle (see CLASS & GOLDSTEIN, 1997; MATA *et al.*, 1998; SPÄTH *et al.*, 2001). The origin of such hydrated magmas in the lithosphere can be considered as the result of metasomatism, which created low solidus and highly enriched lithospheric domains. In Cape Verde the metasomatic agent has been ascribed either to kimberlitic (Sal) or carbonatitic (Santiago) melts based on the detailed study of mantle xenoliths and of lavas (BONADIMAN *et al.*, 2005; MARTINS *et al.*, 2010).

Estimates of temperature and pressure of magmatic segregation using the methods proposed by ALBARÈDE (1992) and GHIORSO *et al.* (1983) give 1309 to 1422 °C and 1.8 to 2.7 GPa (\approx 54 to 84 km) for basaltic magmas and 1412 to 1578 °C and 3.3 to 4.9 GPa (\approx 102 to 152 km) for foiditic magmas. The obtained sub-lithospheric depths of segregation for the majority of magmas support their origin by adiabatic melting of an ascending plume and suggest that the major element composition of plume magmas was not significantly affected by the interaction with lithosphere.

The significant radiogenic isotope variability of Cape Verde magmas has been explained by variable mixing of HIMU, DMM, EM1 and a lower mantle component. So far, it has been of general consensus that Northern Islands (CVN) magmatic sources reflect the contribution of HIMU, DMM and the lower mantle, the EM1 component being restricted to Southern Islands (CVS) sources (GERLACH *et al.*, 1988; DAVIES *et al.*, 1989; KOKFELT *et al.*, 1998; JØRGENSEN & HOLM, 2002; DOUCELANCE *et al.*, 2003; ESCRIG *et al.*, 2005; HOLM *et al.*, 2006; MILLET *et al.*, 2008; BARKER *et al.*, 2009a, b; MARTINS *et al.*, 2010).

Cape Verde EM1-type signatures have been explained by the occurrence in the upper mantle of a megalith(s) of subcontinental lithospheric mantle (SCLM) probably delaminated during the opening of Atlantic ocean. A SCLM origin for the EM1 fingerprints emerged from the geochemical study of lavas (e.g. GERLACH *et al.*, 1988; DOUCELANCE *et al.*, 2003; MILLET *et al.*, 2008; MARTINS *et al.*, 2010) and receive support from a recent geophysical study which imaged a high velocity zone beneath Cape Verde (BEGG *et al.*, 2009). Its

presence beneath Sal, one of the Northern Islands, has been inferred from the study of xenoliths. Indeed, BONADIMAN *et al.* (2005) studied spinel-peridotite xenoliths included in Sal lavas and found evidence for the occurrence of kimberlite-like metasomatism, which was interpreted as caused by the melting of a SCLM domain. More recently, COLORTI *et al.* (2010) presented the results of in situ Os isotope analyses of sulfide grains from the xenoliths. They found Re-depletion model ages mainly ranging from Neoproterozoic to Archean, i.e. compatible with the tectonic history of the western margin of the West African Craton and the corresponding continental margin of Brazil.

Our Sr and Nd isotopic data give some support to these studies suggesting that the presence of SCLM is not restricted to the mantle portions underneath the Southern Islands. Indeed, two of the analyzed Sal samples are characterized by $^{143}\text{Nd}/^{144}\text{Nd}$ neatly lower (0.512770 – 0.512771) than those characterizing CVN or the HIMU component, implying the presence of a more enriched (EM1 ?) component in their source (Fig. 11). This percept is also supported by the fact that these two low $^{143}\text{Nd}/^{144}\text{Nd}$ samples are also characterized by $\text{Ba/Nb} > 10.3$ and $\text{Rb/Nb} > 0.72$ clearly above the values usually reported for lavas with strong HIMU and/or DMM affinities, but compatible with a contribution of the EM1 component (Weaver, 1991; Willbold & Stracke, 2006; 2010).

Thus, our study demonstrating the presence of EM1-type signatures in lavas from Sal, supports that subcontinental lithospheric megaliths, usually considered to be the responsible by the chemical signatures of Southern Cape Verde islands, also exist on the oceanic mantle beneath, at least, one of the Northern Islands.

ACKNOWLEDGEMENTS

This work was written in memory of Paulo Torres, deceased in 1999. It is partially based on a manuscript left by him. This work was funded by Instituto de Investigação Científica e Tropical (IICT), by Centro de Geologia da Universidade de Lisboa (CeGUL), by Centro de Pesquisas Geocronológicas (CPGeo) do Instituto de Geociências do Instituto de Geociências da Universidade de São Paulo (IGc-USP) and by FCT through the research project PLINT (POCTI/CTA/45802/2002). Comments and suggestions of two anonymous reviewers contributed to the improvement of the manuscript.

REFERENCES

- ADAM, J., GREEN, T. H. & SIE, S. H. (1993) – Proton microprobe determined partitioning of Rb, Sr, Ba, Y, Zr, Nd and Ta between experimentally produced amphiboles and silicate melts with variable F content. *Chem. Geol.* **109**:20-49.
- ALBARÈDE, F. (1992) – How deep do common basaltic magmas form and differentiate? *J. Geophys. Res.* **9**: 710997-11009.
- ALI, M.Y., WATTS, A. B., HILL, I. (2003) – A seismic reflection profile study of lithospheric flexure in the vicinity of the Cape Verde Islands. *J. Geophys. Res.* **108**: 2239-2262.
- ANCOCHEA, E., HUERTAS, M. J., HERNÁN, F., BRANDLE, J. L. (2010) – Volcanic evolution of São Vicente, Cape Verde Islands: The Praia Grande landslide. *J. Volcanol. Geotherm. Res.* Doi: 10.1016/J.jvolgeores.2010.08.016
- AZÉMA, J., FOURCADE, E., DE WEVER, P. (1990) – Découverte de Valanginien inférieur à Calpionelles à Maio (République du Cap Vert): discussion de l'âge des sédiments associés aux laves de type MORB de ce secteur de l'Atlantique Central. *C. R. Acad. Sci. Paris* **310** (série II): 277-283.
- BARKER, A. K., HOLM, P. M., PEATE, D. W., BAKER, J. A. (2009a) – Geochemical stratigraphy of submarine lavas (3–5 Ma) from the Flamengos Valley, Santiago, southern Cape Verde Islands. *Journal of Petrology* **50**: 169-193.
- BARKER, A. K., HOLM, P. M., PEATE, D. W., BAKER, J. A. (2009b) – A 5 million year record of compositional variations in mantle sources to magmatism on Santiago, southern Cape Verde archipelago. *Contrib. Mineral. Petrol.* doi: 10.1007/s00410-009-0470-x.
- BEATTIE, P. (1993) – Olivine-melt and orthopyroxene-melt equilibria. *Contrib. Mineral. Petrol.* **115**: 103-111.
- BEBIANO, J. B. (1932) – A geologia do Arquipélago de Cabo Verde. *Comunicações dos Serv. Geol. Portugal* **18**: 1-275.
- BEGG, G. C., GRIFFIN, W. L., NATAPOV, L. M., O'REILLY, S. Y., GRAND, S. P., O'NEILL, C. J., HRONSKY, J. M. A., DJOMANI, Y. P., SWAIN, C. J., DEEN, T. & BOWDEN, P. (2009) – The lithospheric architecture of Africa: Seismic tomography, mantle petrology, and tectonic evolution. *Geosphere* **5** (1), 23-50.
- BONADIMAN, C., BECCALUVA, L., COLORTI, M., SIENA, F. (2005) – Kimberlite-like metasomatism and “garnet signature” in spinel-peridotite xenoliths from Sal, Cape Verde archipelago: relics of a subcontinental mantle domain within the Atlantic Ocean lithosphere? *Journal of Petrology* **46**, 2465-2493.
- BOSSE, V., DOUCELANCE, R., FORNARI, M. & MATA J. (2007) – Temporal evolution of the Cabo Verde archipelago: new constraints from ^{40}Ar - ^{39}Ar data. 2007 Goldschmidt Conference (Cologne). *Geochim. Cosmochim. Acta*, **75** (15S): A110.
- CAHEN, L., SNELLING, N. J., DELHAL, J. & VAIL, J. R. (1984) – Phanerozoic anorogenic igneous activity in Africa. In: *The Geochronology and evolution of Africa*. Colarendon Press. Oxford.
- CALDEIRA, R. & SILVA, L. C. (2008) – Intra-volcanic layered intrusions in Sal island (Cape Verde Archipelago): insights into an ocean island root zone. *Geochim. Cosmochim. Acta*, **72** (12) sup.1, A129.
- CAZENAVE, A., DOMINH, K., RABINOWICZ, M., CEULENEER, G. (1988) – Geoid and depth anomalies over ocean swells and troughs: evidence of an increasing trend of the geoid to depth ratio with age of plate. *J. Geophys. Res.* **93**: 8064-8077.
- CHRISTENSEN, B. P., HOLM, P. M., JAMBON, A., WILSON, J. R. (2001) – Helium, argon and lead isotopic composition of volcanics from Santo Antão and Fogo, Cape Verde Islands. *Chemical Geology* **178**: 127-142.
- CLAGUE, D. A. (1988) – Petrology of ultramafic xenoliths from Loihi Seamount, Hawaii. *Journal of Petrology*, **29** (6), 1161-1186.
- CLAGUE, D. A. & FREY, F. A. (1982) – Petrology and trace element geochemistry of the Honolulu volcanics, Oahu: Implications for the oceanic mantle bellow Hawaii. *Journal of Petrology* **23**: 447-504.
- CLASS, C. & GOLDSTEIN, S. L. (1997) – Plume-lithosphere interactions in the ocean basins: constraints from the source mineralogy. *Earth Planet. Sci. Lett.* **150**: 245-260.
- COLORTI, M., BONADIMAN, C., O'REILLY, S., GRIFFIN, W. L., PEARSON, N. J. (2010) – Buoyant ancient continental mantle embedded in oceanic lithosphere (Sal Island, Cape Verde Archipelago). *Lithos* (in Press).
- COURTNEY, R. C., WHITE, R. S. (1986) – Anomalous heat flow and geoid across the Cape Verde Rise: evidence for dynamic support from a thermal plume in the mantle. *Geophysical Journal of the Royal Astronomical Society* **87**: 815-867.
- DAVIES, G. R., NORRY, M. J., GERLACH, D. C., CLIFF, R. A. (1989) – A combined chemical and Pb-Sr-Nd isotope study of the Azores and Cape Verde hot-spots: the geodynamic implications. Saunders, A. J., Norry, M. J. (Eds.), *Magmatism in the Ocean Basins*. Geological Society Special Publication, vol. **42**: 231-255.
- DE PAEPE & KLERKX, J. (1971) – Peridotite Nodules in nephelinites from Sal (Cape Verde Islands). *Ann. Soc. Geol. Belgique*, **41**, 311-316.
- DE PAEPE, P., KLERKX, J., HERTOGEN, J., PLINKE, P. (1974) – Oceanic tholeiites on the Cape Verde Islands: Petrochemical and geochemical evidence. *Earth and Planet. Sci. Lett.* **22**: 347-354. doi: 10.1016/0012-821X(74)90144-7.
- DOUCELANCE, R., ESCRIG, S., MOREIRA, M., GARIÉPY, C., KURZ, M. D. (2003) – Pb-Sr-He isotope and trace element geochemistry of the Cape Verde Archipelago. *Geochim. Cosmochim. Acta* **67** (717-3), 733.
- DUPRAT, H. I., FRIIS, J., HOLM, P. M., GRANDVUINET, R., SØRENSEN, R. V. (2007) – The volcanic and geochemical development of São Nicolau, Cape Verde Islands: constraints from field and ^{40}Ar / ^{39}Ar evidence. *J. Volcanology and Geothermal Research* **162**, 1-19.
- DYHR, C. T., HOLM, P. M. (2010) – A volcanological and geochemical investigation of Boa Vista, Cape Verde Islands; ^{40}Ar / ^{39}Ar geochronology and field constraints. *J. Volcanology and Geothermal Research* doi: 10.1016/j.jvolgeores.2009.10.010.
- ELLIOT, D. H., FLEMING, T. H., KYLE, P. R., FOLAND, K. A. (1999) – Long-distance transport of magmas in the Jurassic Ferrar large igneous province, Antarctica. *Earth Planet. Sci. Lett.* **167**, 89-104.

- ESCRIG, S., DOUCELANCE, R., MOREIRA, M., ALLÈGRE, C.-J. (2005) – Os-isotope systematics in Fogo Island: Evidence for lower continental crust fragments under the Cape Verde Southern Islands. *Chemical Geology* **219**: 93-113.
- FOEKEN, J. P. T., DAY, S., STUART, F. M. (2009) – Cosmogenic ^{3}He exposure dating of the Quaternary basalts from Fogo, Cape Verdes: Implications for rift zone and magmatic reorganization. *Quaternary Geochronology* **4**: 37-49.
- FOLEY, S. F., JACKSON, S. I., FRYER, B. J., GREENOUGH, J. D. AND JENNER, G. A. (1996) – Trace element partition coefficients for clinopyroxene and phlogopite in an alkaline lamprophyre from Newfoundland by LAM-ICP-MS. *Geochim. Cosmochim. Acta* **60** (4): 629-638.
- FRANCIS, D. & LUDDEN, J. (1995) – The signature of amphibole in mafic alkaline lavas, a study in the Northern Canadian Cordillera. *Journal of Petrology* **36**: 1171-1191.
- GERLACH, D. C., CLIFF, R. A., DAVIES, G. R., NORRY, M., HODGESON, N. (1988) – Magma sources of the Cape Verdes Archipelago: isotopic and trace element constraints. *Geochim. Cosmochim. Acta* **52**: 2979-2992.
- GHIORSO, M. S., CARMICHAEL, I. S. E., RIVERS, M. L. & SACK, R. O. (1983) – The Gibbs free energy of mixing of natural silicate liquids: An expanded regular solution approximation for the calculation of magmatic intensive variables. *Contrib. Mineral. Petrol.* **88**: 260-268.
- GREVEMAYER, I. (1999) – Isostatic geoid anomalies over mid-plate swells in the Central North Atlantic. *Journal of Geodynamics* **28** (1): 41-50.
- GREVEMAYER, I., HELFFRICH, G., FARIA, B., BOOTH-REA, G., SCHNABEL, M., WEINREBE, W. (2009) – Seismic activity at Cadamosto seamount near Fogo Island, Cape Verde – formation of a new ocean island? *Geophysical Journal International* doi: 10.1111/j.1365-246X.2009.04440.x.
- GRIFFITHS J., CANTAGREL J. M., ALVES C. A., MENDES F., SERRALHEIRO A., MACEDO J. R. (1975) – Données radiométriques potassium-argon sur quelques formations magmatiques des îles de l'archipel du Cap Vert. *C. R. Acad. Sci. Paris.* **280** (D): 2429-2432.
- GRUNAU, H. R., LEHNER, P., CLEINTAUR, M. R., ALLENBACK, P., BAKKAR, G. (1975) – New radiometric ages and seismic data from Fuerteventura (Canary Islands), Maio (Cape Verde Islands) and Sao Tome (Gulf of Guinea). In: *Progress in Geodynamics*, Royal Academy of Arts and Sciences, Amsterdam: 90-118.
- GUDFINNSSON, G. H. & PRESNALL, D. C. (2005) – Continuous gradations among primary carbonatitic, kimberlitic, melilititic, basaltic, picritic, and komatiitic melts in equilibrium with garnet lherzolite at 3-8 GPa. *Journal of Petrology*, doi:10.1039/petrology/egi029.
- HANSON, G. N. (1989) – An approach to trace element modeling using a sample igneous system as an example. In: *Reviews in Mineralogy* 21: Geochemistry and Mineralogy of Rare Earth Elements (ed. B.R. Lipin & G.A. McKay), 79-97.
- HART, S. R. (1984) – A large-scale isotope anomaly in the southern hemisphere mantle. *Nature* **309**: 753-757.
- HELFFRICH, G., FARIA, B., FONSECA, J. F. B. D., LODGE, A., KANESHIMA, S. (2010) – Transition zone structure under a stationary hot spot: CapeVerde. *Earth Planet. Sci. Lett.* **289**: 1561614.
- HIRSCHMANN, M. M. & GHIORSO, M. (1994) – Activities of nickel, cobalt, and manganese silicates in magmatic liquids and applications to olivine/liquid and to silicate/metal partitioning. *Geochim. Cosmochim. Acta*, **58** (19): 4109-4126.
- HOLM, P. M., WILSON, J. R., CHRISTENSEN, B. P., HANSEN, L., HANSEN, S. L., HEIN, K. M., MORTENSEN, A. K., PEDERSEN, R., PLESNER, S., RUNGE, M. K. (2006) – Sampling the Cape Verde Mantle Plume: Evolution of Melt Compositions on Santo Antão, Cape Verde Islands. *Journal of Petrology* **47**: 145-189.
- HOLM, P. M., GRANDVUINET, T., FRIIS, J., WILSON, J. R., BARKER A. K., PLESNER, S. (2008) – An ^{40}Ar - ^{39}Ar study of the Cape Verde hot spot: Temporal evolution in a semistationary plate environment. *J. Geophys. Research* **113**, B08201. doi: 10.1029/2007JB005339.
- IRIVINE, T. N. AND BARAGAR W. R. A. (1971) – A guide to the chemical classification of The common volcanic rocks. *Can. J. Earth Sci.* **8**: 523-548.
- JØRGENSEN, J. Ø., HOLM, P. M. (2002) – Temporal variation and carbonatite contamination in primitive ocean island volcanics from São Vicente, Cape Verde Islands. *Chemical Geology* **192**: 249-267.
- KAWASHITA, K. (1972) – O método Rb-Sr em rochas sedimentares. *Unpublished Doctor Thesis*, Instituto de Geociências, Universidade de São Paulo.
- KING, S. D. (2007) – Hotspots and edge-driven convection. *Geology* **35**(3): 223-226.
- KING, S. D., RITSEMA, J. (2000) – African hotspot volcanism: small-scale convection in the upper mantle beneath cratons. *Science* **290**: 1137-1140.
- KOGARKO, L. N. & SENIN, V. G. (1993) – Physicochemical parameters of the oceanic mantle in the Cape Verde Islands. *Geochim. Intern.* **30**(5): 1-8.
- KOKFELT, T. F., HOLM, P. M., HAWKESWORTH, C. J., & PEATE, D. W. (1998) – A lithospheric mantle source for the Cape Verde Island magmatism: trace element and isotopic evidence from the island of Fogo. *Mineralogical Magazine* **62A**: 801-802.
- KUNO, H. (1966) – Lateral variation of basalt magma types across continental margins and island arcs. *Bull. Volcanol.*, **29**: 195-222.
- LASSITER, J. C. (2004) – Role of recycled oceanic crust in the potassium and argon budget of the Earth: Toward a resolution of the “missing argon” problem. *Geochem. Geophys. Geosyst.* **5**, Q11012, doi:10.1029/2004GC000711.
- LATOURRETTE, T., HERUIG, R. L. & HOLLOWAY, J. R. (1995) – Trace element partitioning between amphibole, phlogopite, and basanite melt. *Earth Planet. Sci. Lett.* **135**: 13-30.
- LE BAS, M. J. (1989) – Nephelinitic and basanitic rocks. *Journal of Petrology* **30**: 1299-1312.
- LE BAS, M. J., LE MAITRE, R. W., STRECKEISEN, A. & ZANETTIN, B. (1986) – A chemical classification of volcanic rocks based on the total alkali-silica diagram. *Journal of Petrology* **27**: 745-750.

- LE MAITRE, R. W., STRECKEISEN, A., ZANETTIN, B., LE BAS, M. J., BONIN, B., BATEMAN, P., BELLINI, G., DUDEK, A., EFREMOVA, S., KELLER, J., LAMEYRE, J., SABINE, P. A., SCHMID, R., SØRENSEN, H., WOOLLEY, A. R. (Eds.), (2002) – *Igneous Rocks: A Classification and Glossary of Terms. Recommendations of the International Union of Geological Sciences Subcommission on the Systematics of Igneous Rocks*. Cambridge University Press, 236 pp.
- LECOINTRE, G. (1963) – Sur les terrains sedimentaires de l'île du Sal. *Garcia de Orta, Ser. Geol.* **11**: 275-289.
- LODGE, A., HELFFRICH, G. (2006) – Depleted swell root beneath the Cape Verde Islands. *Geology* **34**: 449-452.
- MADEIRA, J., MUNHÁ, J., TASSINARI, C. C. G., MATA, J., BRUM DA SILVEIRA, A., MARTINS, S. (2005) – K/Ar Ages of Carbonatites from the Island of Fogo (Cape Verde). *Proceedings of the XIV Semana de Geoquímica/ VIII Congresso de Geoquímica dos Países de Língua Portuguesa*, Aveiro, Portugal: 475-478.
- MADEIRA, J., BRUM DA SILVEIRA, A., MATA, J., MOURÃO, C., MARTINS, S. (2008) – The role of mass movements on the geomorphic evolution of ocean islands: examples from Fogo and Brava in the Cape Verde archipelago. *Comunicações Geológicas* **95**: 99-112.
- MADEIRA, J., MATA, J., MOURÃO, C., BRUM DA SILVEIRA, A., MARTINS, S., RAMALHO, R. & HOFFMANN, D. L. (2010) – Volcano-stratigraphic and structural evolution of Brava Island (Cape Verde) from $^{40}\text{Ar}/^{39}\text{Ar}$, U/Th and field constraints. *J. Volcanol. Geotherm Res.* **196**: 219-235.
- MARTINS, S., MATA, J., MUNHÁ, J., MENDES, M. H., MAERSCHALK, C., CALDEIRA, R., MATTIELLI, N. (2010) – Chemical and mineralogical evidence of the occurrence of mantle metasomatism by carbonate-rich melts in an oceanic environment (Santiago Island, Cape Verde). *Mineral. Petrol.* **99**: 43-65.
- MATA, J. (1996) – Petrologia e geoquímica das lavas da ilha da Madeira: implicações para os modelos de evolução do manto terrestre. *Dissertação de Doutoramento* (Univ. Lisboa), 471 p.
- MATA, J. (1998) – in Madeira island alkaline lavas: the influence of magmatic composition. *17th General Meeting of the International Mineralogical Association* (Toronto, Canada), Abstracts and Programs: A9.
- MATA, J. & MUNHÁ, J. (2004) – Madeira Island alkaline lava spinels: petrogenetic implications. *Mineral. Petrol.* **81**: 85-111.
- MATA, J., KERRICH, R., MACRAE, N. D. & WU, T-U. (1998) – Elemental and isotopic (Sr, Nd, and Pb) characteristics of Madeira Island basalts: evidence for a composite HIMU-EM I plume fertilizing lithosphere. *Can. J. Earth Sci.* **35**: 980-997.
- MATA, J., MOREIRA, M., DOUCELANCE, R., ADER, M., SILVA, L. C. (2010) – Noble gas and carbon isotopic signatures of Cape Verde oceanic carbonatites: implications for carbon provenance. *Earth Planet. Sci. Lett.* (in press).
- MCDONOUGH, W. F. & SUN, S.-S. (1995) – The composition of the earth. *Chem. Geol.* **120**: 223-253.
- MCKENZIE, D. & BICKLE, M. J. (1988) – The volume and composition of melt generated by extension of the lithosphere. *Journal of Petrology* **29**: 625-679.
- MENDES, M. H. & SILVA, L. C. (2001) – Xenólitos crustais nas ilhas de Cabo Verde: características petrográficas e química mineral. *Actas VI Congresso de Geoquímica dos PLP/XII Semana de Geoquímica*, Faro, Portugal, 153-156.
- MENDES, M. H., MUNHÁ, J. M., CALDEIRA, R., SILVA, L. C. & PALÁCIOS, T. (2005) – Petrology of peridotitic xenoliths from Sal island, Cape Verde Archipelago. *SAL2005 International Workshop on Ocean Island Volcanism*, 43p.
- MIDDLEMOST, E. A. K. (1975) – The basalt clan. *Earth Sci. Ver.* **11**: 337-364.
- MILLET, M.-A., DOUCELANCE, R., SCHIANO, P., DAVID, K., BOSQ, C. (2008) – Mantle plume heterogeneity versus shallow-level interactions: A case study, the São Nicolau Island, Cape Verde archipelago. *J. Volcanol. Geotherm. Res.* **176**: 265-276. doi: 10.1016/j.jvolgeores.2008.04.003.
- MINSTER, J. F., ALLÈGRE, C. J. (1978) – Systematic use of trace element in igneous processes. Part III: Inverse problem of batch partial melting in volcanic suites. *Contrib. Miner. Petrol.* **68**: 37-52.
- MITCHELL, J. G., LE BAS, M. J., ZIELONKA, J., FURNES, H. (1983) – On dating the magmatism of Maio, Cape Verde Islands. *Earth and Planet. Sci. Lett.* **64**: 61-76.
- MONNEREAU, M., CAZENAVE, A. (1990) – Depth and geoid anomalies over oceanic hotspot swells: a global survey. *J. Geophys. Res.* **95**, 429-438.
- MONTELLI, R., NOLET, G., DAHLEN, F. & MASTERS, G. (2006) – A catalogue of deep mantle plumes: new results from finite-frequency tomography. *Geochem. Geophys. Geosyst.* **7**. doi:10.1029/2006GC001248.
- MORIMOTO, N., FABRIES, J., FERGUSON, A. K., GINZBURG, I.V., ROSS, M., SEIFERT, F. A., ZUSSMAN, J., AOKI, K. & GOTTAIDI, G. (1988) – Nomenclature of pyroxenes. *American Mineralogist*, **73**, 1123-1133.
- MOURÃO, C., MATA, J., MOREIRA, M., DOUCELANCE, R., MADEIRA, J. (2007) – Further Helium isotopic evidence for a lower mantle contribution to the Cape Verde plume. *Geochim. Cosmochim. Acta* **71** (15S): 691.
- MOURÃO, C., MATA, J., DOUCELANCE R., MADEIRA, J., BRUM DA SILVEIRA, A., SILVA, L. C., MOREIRA, M. (2010) – Quaternary extrusive calcio-carbonatite volcanism in Brava Island (Cape Verde): A nephelinite-carbonatite immiscibility product. *J. Afr. Earth Sci.* **56**: 59-74.
- MÜLLER, R. D., SDROLIAS, M., GAINA, C., ROEST, W. R. (2008) – Age, spreading rates, and spreading asymmetry of the world's ocean crust. *Geochem. Geophys. Geosyst.* **9**, Q04006.
- MUNHÁ, J., SILVA, L. C., PALÁCIOS, T. & TORRES, P.C. (1991) – Origin of $\text{CaFe}^{3+}\text{AlSiO}_6$ – rich pyroxenes in olivine-nephelinites and olivine-melilites from Sal, Cape Verde Islands. *Garcia de Orta, Ser. Geol.*, **14**, 15-27.
- PATRIAT, M., LABAILS, C. (2006) – Linking the Canary and Cape-Verde Hot-Spots, Northwest Africa. *Marine Geophys. Res.* **27**(3): 201-215. doi: 10.1007/s11001-006-9000-7.
- PIM, J., PEIRCE, C., WATTS, A. B., GREVEMEYER, I., KRABBENHOEFT, A. (2008) – Crustal structure and origin of the Cape Verde Rise. *Earth Planet. Sci. Lett.* **272**: 422-428. doi: 10.1016/j.epsl.2008.05.012.

- PLESNER, S., HOLM, P. M., WILSON, J. R. (2002) – ^{40}Ar - ^{39}Ar geochronology of Santo Antão, Cape Verde Islands. *J. Volcanol. Geotherm. Res.* **120**: 103-121.
- POLLITZ, F. F. (1991) – Two-stage model of African absolute motion during the last 30 million years. *Tectonophysics* **194**: 91-106.
- PUTIRKA, K. (2008) – Excess temperatures at ocean islands: Implications for mantle layering and convection. *Geology* **36** (4), 283-286, doi:10.1130/G24615A.
- RAMALHO, R., HELFFRICH, G., SCHMIDT, D. N., VANCE, D. (2010a) – Tracers of uplift and subsidence in the Cape Verde archipelago. *J. Geol. Soc. London* **167**: 519-538.
- RAMALHO, R. S., HELFFRICH, G., COSCA, M., VANCE, D., HOFFMAN, D. & SCHMIDT, D. N. (2010b) – Vertical movements of ocean island volcanoes: insights from a stationary plate environment. *Marine Geology* doi: 10.1016/j.margeo.2010.04.009 (in press).
- ROEDER, P. L. & EMSLIE, R.F. (1970) – Olivine-liquid equilibrium. *Contrib. Mineral. Petrol.* **29**: 275-289.
- RYABCHIKOV, J. D., NTAFLOS, T., KURAT, G. & KOGARKO, L. N. (1995) – Glass-bearing xenoliths from Cape Verde: Evidence for a hot rising mantle jet. *Min. Petrol.* **55** (4): 217-237.
- SATO, K., TASSINARI, C. C. G., KAWASHITA, K., PETRONILHO, L. (1995) – O método geocronológico Sm-Nd no IGc – USP e suas aplicações. *Anais da Academia Brasileira de Ciências*, **3** (67): 313-336.
- SCHUBERT, G., TURCOTTE, D. L., OLSON, P. (2001) – *Mantle Convection in the Earth and Planets*, Cambridge University Press, Cambridge: 940 pp.
- SERRALHEIRO, A. (1968) – Formações Sedimentares do Arquipélago de Cabo Verde. *Junta de Investigações do Ultramar*, Lisboa.
- SERRALHEIRO, A. (1970) – A geologia da Ilha de Maio (Cabo Verde). *Junta de Investigações do Ultramar*, Lisboa: 103 pp.
- SERRALHEIRO, A. (1976) – A geologia da ilha de Santiago. *Bol. Museu Lab. Mineral. Geol. Fac. Ciências de Lisboa* **14**: 218 pp.
- SHAW, S. J., HEIDELBACH, F. & DINGWELL, D. B. (2006) – The origin of reaction textures in mantle peridotite xenoliths from Sal Island, Cape Verde: the case for ‘metasomatism’ by the host lava. *Contrib. Miner. Petrol.* **151**: 681-697.
- SILVA, L. C. (1991) – Petrologia e geoquímica de complexos subvulcânicos anelares – Ilha da Sal, República de Cabo Verde. *3.º Congresso Brasileiro de Geoquímica / 1.º Congresso de Geoquímica dos Países de Língua Portuguesa*, São Paulo, Brasil, I: 98-99.
- SILVA, L., SERRALHEIRO, A., MACEDO, J., GOMES, A. & TORRES, P. (1990) – *Carta Geológica de Cabo Verde, Ilha do Sal, na escala de 1/25 000 (folhas 1-2)*. Instituto Investigação Científica Tropical-Instituto de Cooperação Económica, Lisboa.
- SILVA, L. C., SERRALHEIRO, A., MACEDO, J. R., GOMES, A. MOTA & TORRES, P. T. (1993) – Fosfatização de rochas basálticas da ilha do Sal, Arquipélago de Cabo Verde. *Garcia de Orta, Ser. Geol.* **15** (1-2): 1-22.
- SILVA, L. C., SERRALHEIRO, A., TORRES, P. C., MACEDO, J. R., MENDES, M. H. & MOTA GOMES, A. (2002) – “Geologia da Salina de Pedra Lume, Ilha do Sal, Cabo Verde”. *Garcia de Orta, Ser. Geol.* **18** (1-2): 15-18.
- SILVER, P., RUSSO, R., LITHGOW-BERTELLONI, C. (1998) – Coupling of South American and African plate motion and plate deformation. *Science* **279**: 60-63.
- SPATH, A., LE ROEX, A. P. & OPIYO-AKECH, N. (2001) – Plume – lithosphere interaction and the origin of continental rift-related alkaline volcanism. The Chyulu Hills Volcanic Province, Southern Kenya. *Journal of Petrology* **42**: 765-787.
- STILLMAN, C. J., FURNES, H., LE BAS, M. J., ROBERTSON, A. H. F., ZIELONKA, J. (1982) – The geological history of Maio, Cape Verde Islands. *Journal of the Geological Society of London* **139**: 347-361.
- SUN, S. S. & McDONOUGH, W. F. (1989) – Chemical and isotopic systematics of oceanic basalts: Implications for mantle composition and processes. In: Saunders, A. D. and Norry, M. J. (eds) – *Magmatism in the ocean basins*, Geological Society Spec. Publ., **42**: 313-345.
- TORRES, P. C. (1998) – *Geologia e petrogénese das formações vulcânicas da Ilha do Sal, Arquipélago de Cabo Verde*. Thesis (Phd eq.), IICT, Lisboa, 212p.
- TORRES, P. C., MADEIRA, J., SILVA, L. C., BRUM DA SILVEIRA, A., SERRALHEIRO, A. & MOTA GOMES, A. (1997) – Carta geológica das erupções históricas da ilha do Fogo: revisão e actualização. *Proceedings of the 1st International Symposium “A erupção vulcânica de 1995 na ilha do Fogo, Cabo Verde”*, published by Instituto de Investigação Científica Tropical and Ministério da Ciência e Tecnologia: 119-132.
- TORRES, P. C., MADEIRA, J., SILVA, L. C., BRUM DA SILVEIRA, A., SERRALHEIRO, A. & MOTA GOMES, A. (1998a) – Carta geológica da ilha do Fogo (República de Cabo Verde): erupções históricas e formações enquadrantes. Published by Laboratório de Tectonofísica e Tectónica Experimental (LATTEX), Lisboa, Portugal: 1 sheet at the 1:25.000 scale.
- TORRES, P. C., SILVA, L. C., MENDES, M. H., MUNHÁ, J. & MATA, J. (1998b) – On the genesis of the Cape Verde islands: tectonic influence. *V Congresso Nacional de Geologia (Lisboa). Comun. Inst. Geol. Min. (Portugal)* **84** (I): B168-B169.
- TORRES, P. C., SILVA, L. C., SERRALHEIRO, A., TASSINARI, C., MUNHÁ, J. (2002a) – Enquadramento geocronológico pelo método K/Ar das principais sequências vulcânicas-estratigráficas da Ilha do Sal – Cabo Verde. *Garcia de Orta, Ser. Geol.* **18** (1-2): 9-13.
- TORRES, P. C., SILVA, L. C., SERRALHEIRO, A., MENDES, M. H., MACEDO, J. R. & MOTA GOMES, A. (2002b) – Geologia da ilha do Sal. *Comunicações do IICT*, **10**: 57p.
- UBALDO, M. L., SILVA, L. C. & TORRES, P. C. (1991) – Contribuição geológica e micropalontológica para o conhecimento do “Complexo eruptivo antigo” da ilha do Sal, Arquipélago de Cabo Verde. *Garcia de Orta, Ser. Geol.* **14** (1, 2): 9-14.
- WALLACE, M. E & GREEN, D. H. (1991) – The effect of bulk rock composition on the stability of amphibole in the upper mantle: Implications for solidus positions and mantle metasomatism. *Mineral. Petrol.* **44**: 1-19.
- WATSON, S. & MCKENZIE, D. (1991) – Melt generation by plumes: A study of Hawaiian volcanism. *Journal of Petrology*, **32**: 501-537.
- WATSON, E. B. (1979) – Zircon saturation in felsic liquids: experimental results and applications to trace element geochemistry. *Contrib. Mineral. Petrol.* **70**: 407-419.

- WEAVER, B. L. (1991) – The origin of ocean island basalt end-member compositions: trace element and isotopic constraints. *Earth and Planet. Sci. Lett.* **104**: 381-397.
- WILBOLD, M. & STRACKE, A. (2006) – Trace element composition of mantle end-members: Implications for recycling of oceanic and upper and lower continental crust. *Geochem. Geophys. Geosyst.* **7** (4), Q04004, doi:10.1029/2005GC001005.
- WILBOLD, M. & STRACKE, A. (2010) – Formation of enriched mantle components by recycling of upper and lower continental crust. *Chemical Geology*, doi:10.1016/j.chemgeo.2010.06.005.
- WILLIAMS, C. A., HILL, I. A., YOUNG, R., WHITE, R. S. (1990) – Fracture zones across the Cape Verde Rise, N.E. Atlantic. *J. Geol. Soc.* **147**: 851-857.
- ZAZO, C., GOY, J., DABRIO, C. (2007) – Quaternary marine terraces on Sal Island (Cape Verde archipelago). *Quaternary Science Reviews* **26**: 876-893.
- ZHAO, D. (2007) – Seismic images under 60 hotspots: search for mantle plumes. *Gondwana Research* **12**: 335-355.
- ZINDLER, A. & HART, S. (1986) – Chemical geodynamics. *Ann. Rev. Earth Planet. Sci.* **14**: 493-571.

